Brief Report

Induced Navier's Slip with CNTS on a Stretching/Shrinking Sheet under the Combined Effect of Inclined MHD and Radiation

Mahabaleshwar Ulavathi. Shettar [1], Mahesh Rudraiah [1], Jean Bragard [2] and David Laroze [3,*]

1. Department of Studies in Mathematics, Davangere University, Davangere 577007, India
2. Department of Physics and Applied Mathematics, School of Sciences, University of Navarra, 31008 Pamplona, Spain
3. Instituto de Alta Investigación, CEDENNA, Universidad de Tarapacá, Casilla 7D, Arica 1000000, Chile
* Correspondence: dlarozen@uta.cl

Abstract: The present article investigates viscous fluid flow's heat and mass transfers over a stretching/shrinking sheet using the single and multi-wall carbon nanotube models. The analysis considers the effects of thermal radiation, induced slip, mass transpiration, and inclined magnetic force. The effect of the carbon nanotube model on fluid flow has not been considered in previous studies. By exploiting the similarity variable, the governing nonlinear partial differential equations are converted into nonlinear ordinary differential equation. The derived equations are solved analytically, and we obtained an exact solution for the velocity and energy conservation equation. The physical parameters of interest such as induced slip parameter, suction/injection, magnetic field, thermal radiation, and shear stress are analyzed and presented graphically. In particular, we show that the fluid flow in a single wall carbon nanotube transfers more energy than the multivalued nanotubes.

Keywords: heat and mass transfer; CNTs; induced slip; inclined MHD; mass transpiration; radiation; stretching/shrinking sheet

1. Introduction

During the last few decades, many studies have been devoted to the thermal conductivity of nanofluids. Most nanofluid research focuses on understanding their physical characteristics to improve heat transfer in various industrial applications, including nuclear reactors, power production, transportation, paper cooling and drying, electronics, medical, and food. In 1991, Iijima [1] discovered cylindrical carbon atom structures ranging from 1 to 100 nanometers, known as carbon nanotubes (CNTs in short). Carbon nanotubes can be classified as single-wall (SWCNTs) or multi-wall (MWCNTs). CNTs offer great potential as nanocontainers for storing gas and nano pipes for moving fluid because of their perfect hollow cylindrical form and superior mechanical strength. These CNTs' properties inspired other researchers, who conducted a numerical analysis of single and multi-wall CNTs dispersion in various carrier fluids.

The effect of carbon nanotubes (CNT) on the MHD of Newtonian fluid flow across a nonlinear stretching sheet has been investigated by Mahabaleshwar et al. [2] and others [3–8]. A study comparing the flows of SWCNT and MWCNT saturated with water over a curved surface by Khan et al. [9]. Sneha et al. [10] examined the influence of carbon nanotubes on a non-Newtonian fluid flow with the impact of radiation and mass transpiration over a stretching/shrinking sheet. Nadeem et al. [11] examined the heat transfer analysis of SWCNT-MWCNT in three different base fluids. The influence of CNTs on a radioactive MHD fluid flow in the prances of the heat source/sink over a stretching/shrinking flat plate was studied previously by Mahabaleshwar et al. [12].

Numerous engineering and medical devices use electrically conducting fluids set in motion by a magnetic force through MHD boundary layer fluxes. This magnetic field

produces a Lorentz force that opposes the fields and currents. MHD has been shown crucial in various fluid flow scenarios, with applications in the pharmaceutical industry, energy generation, etc. Noteworthy are the high-temperature processes where thermal radiation significantly impacts boundary layer flow. These high-temperature effects have been considered in a range of engineering applications. The role of heat radiation is crucial for ensuring product quality because it has a direct impact on cooling rates.

To explore the turbulent convection heat transfer of hybrid nanofluid, Hayat et al. [13] examined the effect of radiation on second-grade fluid-induced two-dimensional Blasius flow and heat transport. Devi and Devi [14] examined numerically the impact of Lorentz force on an ejected from a stretched sheet. Bhattacharyya and Layek [15] investigated the forced convection flow with the influence of radiation via a porous shrinking plate. Bhattacharyya et al. [16] investigated the effect of micro polar through viscous flow and heat transmission of shrinking porous surfaces on viscous flow and heat transmission.

Numerous industrial processes are closely dependent on viscous fluid flows. Let us cite, without being exhaustive, the manufacture of plastic sheets, paper, the spinning of fibers, etc., that are performed by a sheet that is contracting or expanding with mass suction or injection. Miklavcic and Wang [17] were the first to discover the existences of the dual nature solution in a particular range of mass suction rate over a gas flow in a linearly shrinking sheet. Later this problem was extended for a shrinking sheet with a power law velocity [18].

One characteristic that distinguishes micro and nanoscale fluid flow from their macroscale counterparts is that the wall-slip effect frequently becomes essential. Overlooking them might result in completely wrong predictions. When used with appropriate slip conditions on the boundary, the Navier–Stokes equation was demonstrated in Wu [19] to produce accurate results for nano/macroscale gas flows. Wang [20] used Maxwell's first order slip flow model to examine the stretching sheet problem. Using a second-order slip flow model created by Wu [19], Fang et al. [21,22] studied the wall-slide effect on fluid flow over a shrinking/stretching sheet and discovered that the flow solutions heavily depend on the first and second order slip coefficients. Wu [23] used the induced slip for the viscous gas flow and he identified that mass-suction induced slip may even play a major flow-driven function by completely reversing the flow direction of nearby gases, thus creating a flow against the sheet motion. The moving sheet's flow-driven action is enhanced by mass-injection-caused slip. Wu [24] was the first to propose the induced slip, and he analyzed heat effect and mass transfer of the gas flow in the stretching/shrinking sheet setting and he found out that velocity caused by mass transfer slip can significantly alter gas flow velocity, resulting in non-negligible changes in temperature distribution and wall heat flux via thermal convection.

Due to its crucial impact on the quality control of the production processes for polymers, paper, glass, and metallurgy, heat transfer of the viscous fluid flow in a moving has attracted much interest in recent years. Crane [25] found accurate similarity solutions for the temperature and velocity fields in a 2-D steady viscous fluid flow across a stretched sheet. Further, it is enhanced by including mass transpiration, surface temperature, and stretching sheet; all these additional effects have been studied in the following references [26–28].

It is well-known that any material at a temperature above absolute zero spontaneously releases energy through the thermal radiation mechanism. Fluid flow having a significant radiation effect is employed in various industrial applications, including spacecraft, nuclear power plants, missiles, and aircraft propulsion systems. Many scientists have turned to the radiation effect to discover the peculiarities of liquid motion. Recently Mahabaleshwar et al. [29] showed the effect of radiation on the Graphene Casson Nanofluid and the effect of CNTs modeled through a Newtonian fluid flow formulation. Recently Anusha et al. [30], Vishalaksi et al. [31], Senha et al. [32] and several researchers in the following references [33–40] have discussed the flow of several nano liquids along various types of surfaces.

The present paper aims at examining the fluid flow in SWCNT and MWCNT with the impact of the induced slip and inclined MHD. It analyzes the heat transfer rate by varying the thermal radiation over a stretching/shrinking sheet. The paper's novelty lies in introducing the CNTs models on an induced slip for the stretching/shrinking sheet. The outcomes have potential technological applications in liquid-based systems involving stretchable/shrinkable fabrics, especially drawing, annealing, and thinning of metallic wires, continuous stretching/shrinking, rolling, manufacturing of plastic film, and artificial fibers in Bioengineering. The effect of thermal radiation in this type of problem-inclined MHD is also new. The set of nonlinear PDEs is converted into a collection of nonlinear ODEs by employing the appropriate similarity transformation, as it is standard for the study of boundary layers. Blasius and Prandtl developed the method at the beginning of the twentieth century (see Schlichting [41]). The resulting ordinary differential equations are solved analytically. We obtain an explicit dual nature exact solution for both the stretching/shrinking sheet. The results are analyzed using graphical methods to study the importance of the physical parameters.

The most important results from the technological aspect are the computation of the Nusselt number (heat transfer) and the skin friction (viscous drag at the surface) as a function of the parameter of the problem. The novelty of the present paper lies in the inclusion into the model of an applied magnetic field and the presence of heat transfer through radiation (not only conduction and convection) as it is standard in other studies of the nanofluidic systems (see Khan et al. [42]).

2. The Theoretical Models and Solutions

Let us describe the two-dimensional viscous Newtonian fluid flow over single and multi-wall carbon nanotube over a stretching/shrinking sheet. The underneath sheet moves horizontally at a fixed given speed. Similarly, gases are supplied from the wall into the system in a normal direction. The schematic setup is shown in Figure 1.
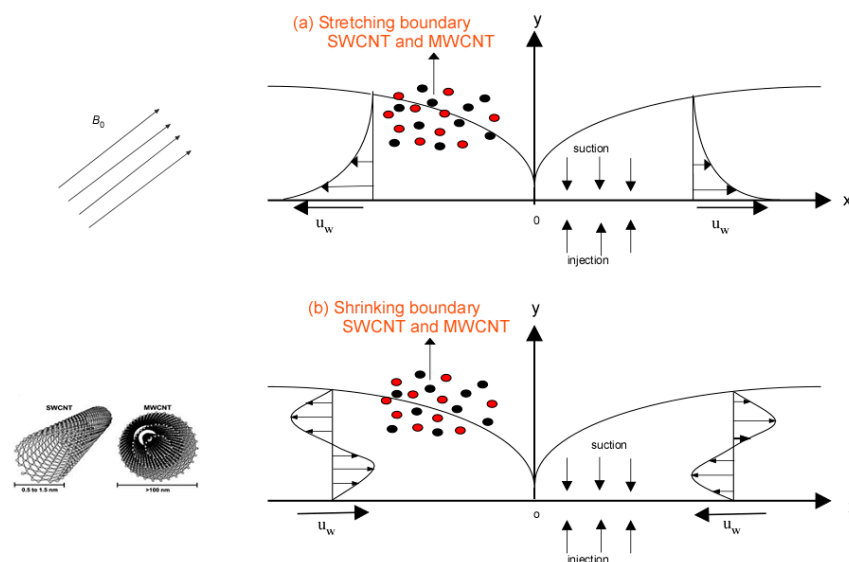

Figure 1. Simplified representation of the physical problem.

The governing equations for the fluid flow over the plate are as follows [23,24,42]:

$$\frac{\partial u}{\partial x} + \frac{\partial v}{\partial y} = 0, \tag{1}$$

$$u\frac{\partial u}{\partial x} + v\frac{\partial u}{\partial y} = -\frac{1}{\rho}\frac{\partial p}{\partial x} + v_{nf}\left[\frac{\partial^2 u}{\partial x^2} + \frac{\partial^2 u}{\partial y^2}\right] - \frac{\sigma_{nf}B_0{}^2}{\rho_{nf}}\sin^2(\tau)u, \tag{2}$$

$$u\frac{\partial v}{\partial x} + v\frac{\partial v}{\partial y} = -\frac{1}{\rho}\frac{\partial p}{\partial y} + v_{nf}\left[\frac{\partial^2 v}{\partial x^2} + \frac{\partial^2 v}{\partial y^2}\right] - \frac{\sigma_{nf}B_0^2}{\rho_{nf}}\sin^2(\tau)v, \tag{3}$$

$$u\frac{\partial T}{\partial x} + v\frac{\partial T}{\partial y} = \alpha_{nf}\frac{\partial^2 T}{\partial y^2} - \frac{1}{(\rho Cp)_{nf}}\frac{\partial q_r}{\partial y}. \tag{4}$$

Following Blasius and others, the corresponding boundary conditions are provided by:

$$\begin{cases} u(x,0) = u_w + u_{slip}, & v(x,0) = v_w, & T(x,0) = T_w \text{ at } y = 0, \\ u(x,\infty) = 0, & T(x,\infty) = T_\infty, & as \ y \to \infty, \end{cases} \tag{5}$$

where u and v are the velocity component in the x and y direction, $u_w = \pm ax$ represents the momentum of the fluid with speed a. v_w is the wall mass flux of the velocity and u_{slip} is the velocity of gas slip at the stretching surface which is provided as follows (see [42]):

$$u_{slip} = b_s\,\lambda\,\frac{\partial u}{\partial y} - c_s\,\lambda^2\,\frac{\partial^2 u}{\partial y^2} + \frac{4\,M}{\alpha\,\rho\,\overline{v}}u_w\ , \tag{6}$$

where

$$b_s = 2(3 - \alpha\,f^3)/(3\alpha) - (1 - f^2)/K_n \tag{7}$$

and

$$c_s = f^4/4 + (1 - f^2)/(2K_n^2) \tag{8}$$

where K_n is the Knudsen number, $M = \rho\,v_w$ is the mass flux at the wall, and the slip velocity at the stretched sheet can be expressed by:

$$u_{slip} = b_s\,\lambda\,\frac{\partial u}{\partial y} - c_s\lambda^2\frac{\partial^2 u}{\partial y^2} \pm \Gamma_1 ax, \tag{9}$$

where $\Gamma_1 = 4v_w/(\alpha\,v)$ the non-dimensional mass transfer is induced slip parameter.

By using the Rosseland's approximation, the radiative heat flux is provided as,

$$q_r = -\frac{4\sigma^*}{3\kappa^*}\frac{\partial T^4}{\partial y}, \tag{10}$$

where σ^* is the Stefan–Boltzmann constant and κ^* is the spectral absorption coefficient. Using Taylor series expansion, T^4 is approximated to $T^4 \cong -3T_\infty^4 + 4T_\infty^4 T$. Therefore

$$\frac{\partial q_r}{\partial y} = -\frac{16\sigma^* T_\infty^3}{3\kappa^*}\frac{\partial^2 T}{\partial y^2} \tag{11}$$

2.1. The Expression and Thermo-Physical Properties of the CNTs

The expressions for the CNTs thermophysical properties used in the present studies are a compilation from different previous studies as shown in Figure 2. The dynamical viscosity of the nanofluidic suspensions is approximated by the Einstein relation (see Alexander and Michael [43]). The equivalent thermal conductivity is taken form the study of Xue in [44].
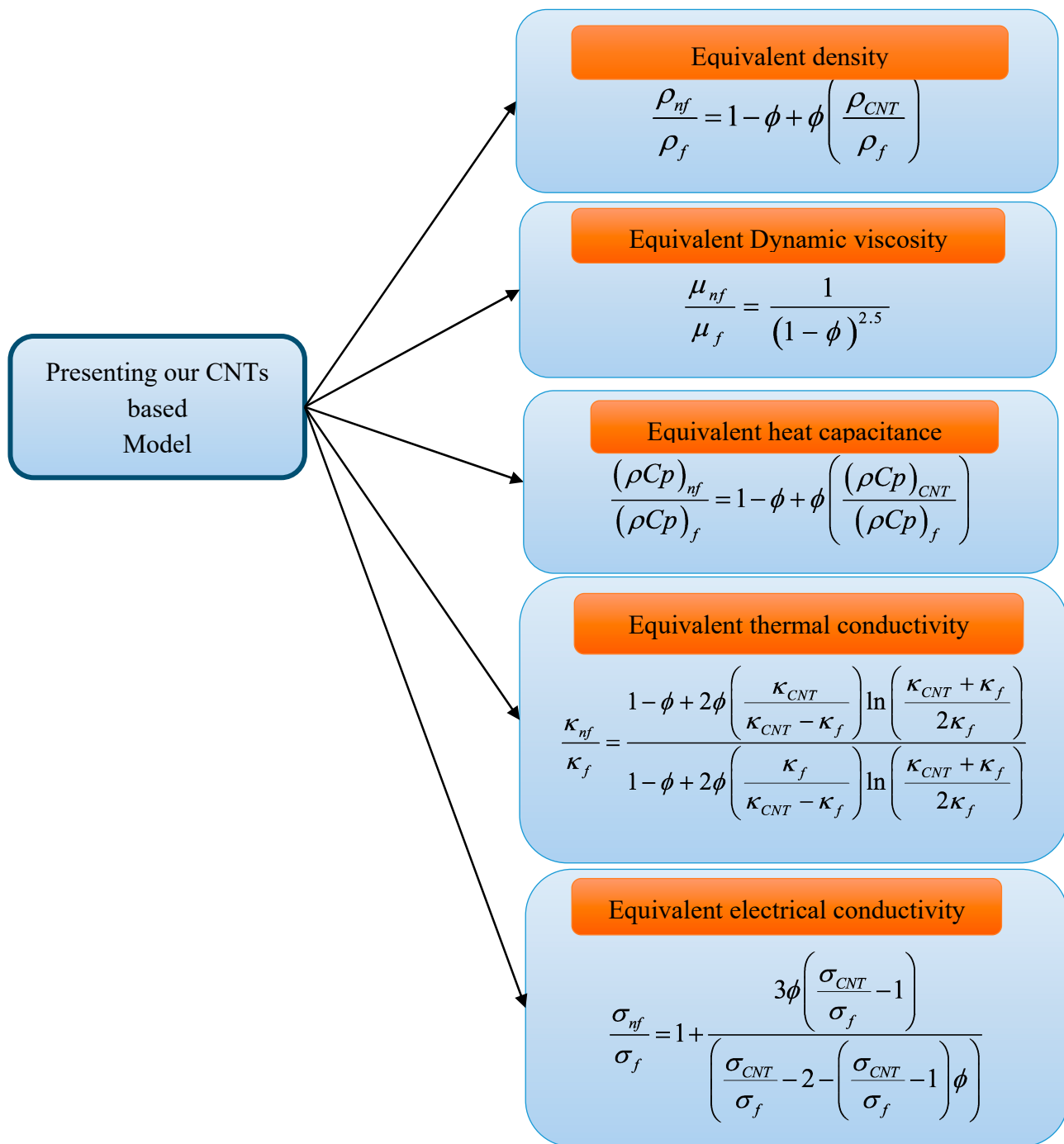
Equivalent density

$$\frac{\rho_{nf}}{\rho_f} = 1 - \phi + \phi\left(\frac{\rho_{CNT}}{\rho_f}\right)$$

Equivalent Dynamic viscosity

$$\frac{\mu_{nf}}{\mu_f} = \frac{1}{(1-\phi)^{2.5}}$$

Equivalent heat capacitance

$$\frac{(\rho Cp)_{nf}}{(\rho Cp)_f} = 1 - \phi + \phi\left(\frac{(\rho Cp)_{CNT}}{(\rho Cp)_f}\right)$$

Equivalent thermal conductivity

$$\frac{\kappa_{nf}}{\kappa_f} = \frac{1 - \phi + 2\phi\left(\dfrac{\kappa_{CNT}}{\kappa_{CNT} - \kappa_f}\right)\ln\left(\dfrac{\kappa_{CNT} + \kappa_f}{2\kappa_f}\right)}{1 - \phi + 2\phi\left(\dfrac{\kappa_f}{\kappa_{CNT} - \kappa_f}\right)\ln\left(\dfrac{\kappa_{CNT} + \kappa_f}{2\kappa_f}\right)}$$

Equivalent electrical conductivity

$$\frac{\sigma_{nf}}{\sigma_f} = 1 + \frac{3\phi\left(\dfrac{\sigma_{CNT}}{\sigma_f} - 1\right)}{\left(\dfrac{\sigma_{CNT}}{\sigma_f} - 2 - \left(\dfrac{\sigma_{CNT}}{\sigma_f} - 1\right)\phi\right)}$$

Figure 2. Summary of the CNTs based model.from [32].

For the equivalent electrical conductivity, the Maxwell model is used where the electrical conductivity of the nanofluid (κnf), the electrical conductivity of nanoparticles (κnp) and of the base fluid (κf), is taken into account (see Chereches and Minea [45]). All the expressions for the nanofluidic thermophysical properties are dependent of the particle volume fraction (φ) and can be summarized as:

2.2. Similarity Variables

In order to simplify the equations, we propose the following similarity transformations applied to the main governing equations.

$$\psi(x,y) = x\sqrt{va}f(\eta), \quad \Theta(\eta) = \frac{T - T_\infty}{T_w - T_\infty}, \quad \eta = \sqrt{\frac{a}{v}}y, \tag{12}$$

where the stream function is represented as ψ and it is related to u and v as follows:

$$u(x,y) = \frac{\partial \psi}{\partial y} = axf_\eta(\eta),$$

and

$$\text{v}(x,y) = -\frac{\partial \psi}{\partial x} = -\sqrt{va}f(\eta),$$

at this stage, by using similarity transformations, and the thermophysical expression's the Equations (1)–(4) are further simplified. By solving Equations (2)–(4) using Equation (12), we obtain the following results:

$$A_1 f_{\eta\eta\eta}(\eta) - A_5 M \sin^2(\tau)f_\eta(\eta) + A_2\left[f(\eta)f_{\eta\eta}(\eta) - f_\eta(\eta)^2\right] = 0, \tag{13}$$

$$(A_4 + N_r)\theta_{\eta\eta}(\eta) + A_3 \text{Pr}f(\eta)\theta_\eta(\eta) = 0, \tag{14}$$

with the associated boundary conditions,

$$f(0) = -\frac{v_w}{\sqrt{va}} = \Gamma_2, \quad f_\eta(0) = \pm(1 + \Gamma_1) + \Lambda_1 f_{\eta\eta}(0) + \Lambda_2 f_{\eta\eta\eta}(0), \quad f_\eta(+\infty) \to 0, \tag{15}$$

$$\theta(0) = 1, \quad \theta(\infty) = 0 \tag{16}$$

where

$$\Lambda_1 = b_s\lambda\sqrt{\frac{a}{v}}$$

$$\Lambda_2 = -c_s\lambda^2\frac{a}{v},$$

$Nr = \frac{16\sigma^* T_\infty^3}{3\kappa_f k^*}$ represents the radiation number,

$\text{Pr} = \frac{v_f}{\alpha}$ stands for the Prandtl number,

$M = \frac{\sigma_f B_0^2}{a\rho_f}$ quantifies the magnetic field.

2.3. Exact Solution for Velocity Equation

The analytical solution to Equation (13) subject to boundary conditions Equations (15)–(17) is provided by:

$$f(\eta) = \Gamma_2 + \frac{(\Gamma_1 + 1)\{1 - \exp(-\alpha\eta)\}}{\alpha[1 + \Lambda_1\alpha - \Lambda_2\alpha^2]} \tag{17}$$

where $\alpha > 0$ represents the solution of an algebraic equation of fourth order. By considering $\tau = \frac{\pi}{2}$ then $\sin(\tau) = 1$. Hence, the algebraic equation α can be written as follows:

$$p\alpha^4 + q\alpha^3 + r\alpha^2 + s\alpha + w = 0, \tag{18}$$

where

$$
\begin{aligned}
p &= A_1\Lambda_2, \\
q &= -(A_1\Lambda_1 + A_2\Gamma_2\Lambda_2), \\
r &= -(A_1 + A_5M\Lambda_2 - A_2\Gamma_2\Lambda_1), \\
s &= (A_5\Lambda_1 M + A_2\Gamma_2), \\
&\text{and} \\
w &= (A_5M \pm A_2(1 + \Gamma_1)).
\end{aligned}
$$

In the above expression for w we take the positive sign for the stretching case and the negative sign for the shrinking case. The roots of the fourth order polynomial Equation (18) are computed and provided explicitly in Appendix A at the end of the paper.

The non-dimensional shear stress function is provided as

$$
f_{\eta\eta}(\eta) = -\frac{(1+\Gamma_1)\alpha Exp[-\alpha\eta]}{1 + \Lambda_1\alpha - \Lambda_2\alpha^2}
$$

2.4. Solution for the Temperature Equation

The Equation (14) can be further modified with the aid of Equation (18), and by introducing a new parameter $t = \frac{\text{Pr}}{\alpha^2} Exp[-\alpha\eta]$, it transforms into

$$
t\Theta_{tt}(t) + (m + nt)\Theta_t(t) = 0, \tag{19}
$$

Subjected to the following boundary conditions:

$$
\Theta\left(\frac{\text{Pr}}{\alpha^2}\right) = 1 \quad \text{and} \quad \Theta(0) = 0. \tag{20}
$$

where

$$
m = \left\{1 - \frac{A_3\text{Pr}\Gamma_2}{\alpha(A_4 + Nr)} - \frac{A_3pr(1+\Gamma_1)}{\alpha^2(A_4 + Nr)(1 + \Lambda_1\alpha - \Lambda_2\alpha^2)}\right\}, \quad \text{and} \quad n = \frac{A_3(1+\Gamma_1)}{(A_4 + Nr)(1 + \Lambda_1\alpha - \Lambda_2\alpha^2)}.
$$

subject to boundary conditions, Equation (18) can be straightforwardly integrated twice,

$$
\theta(t) = \frac{c_1}{n^{1-m}} \int_0^{nt} \sigma^{a-1} e^{-\sigma} d\sigma + c_2, \tag{21}
$$

By imposing the boundary conditions (20), i.e., $\Theta\left(\frac{\text{Pr}}{\alpha^2}\right) = 1$ and $\Theta(0) = 0$. The constants in Equation (21) are provided by:

$$
c_1 = \frac{n^{1-m}}{\Gamma\left(1 - m, \frac{n\text{Pr}}{\alpha^2}\right) - \Gamma(1 - m, 0)}, \tag{22}
$$

$$
c_2 = -\frac{\Gamma(1 - m, 0)}{\Gamma\left(1 - m, \frac{n\text{Pr}}{\alpha^2}\right) - \Gamma(1 - m, 0)}, \tag{23}
$$

Thus, $\theta(t)$ is obtained in the following exact form:

$$
\Theta(t) = \frac{\Gamma[1 - m, 0] - \Gamma[1 - m, nt]}{\Gamma[1 - m, 0] - \Gamma\left[1 - m, \frac{n\text{Pr}}{\alpha^2}\right]}, \tag{24}
$$

In terms of the similarity variable η, Equation (24) transforms back into:

$$\Theta(\eta) = \frac{\Gamma[1-m,0] - \Gamma\left[1-m, \frac{n\mathrm{Pr}}{\alpha^2}\mathrm{Exp}[-\alpha\eta]\right]}{\Gamma[1-m,0] - \Gamma\left[1-m, \frac{n\mathrm{Pr}}{\alpha^2}\right]} \tag{25}$$

In the next section, we analyze the behavior of these analytical expressions.

3. Results and Discussion

The calculation of the skin friction Cf is important to evaluate the frictional drag that is applied on an object immersed in a fluid. One usually uses the Newton formula:

$\tau_w = \mu_{nf}\left(\frac{\partial u}{\partial y}\right)_{y=0}$ is known as surface shear stress

By imposing the similarity transformation, we obtain

$$Re_x^{1/2}C_f = 2 * A_2 * F''(0),$$

In the present article we discuss the analytical dual branch solution for the fluid flow in flow over single and multi-wall carbon nanotubes in a stretching and shrinking case with the presence of the inclined magnetic field and thermal radiation. The following section presents graphic results for different value of Γ_1, Γ_2, M, N_r and P_r. The thermophysical properties of CNT are shown in Table 1 and the Prandtl number for water is kept as 6.2.

Table 1. Physical properties of the base fluid and the CNTs taken from [32,42].

Physical Properties	Fluid Phase (Water)	SWCNT	MWCNT
$C_p\,(\mathrm{J/kgK})$	4179	425	796
$\rho\left(\mathrm{Kg/m^3}\right)$	997.1	2600	1600
$\kappa(\mathrm{W/mK})$	0.613	6600	3000
$\sigma(\Omega/\mathrm{m})^{-1}$	0.05	48,000,000	38,000,000

The demonstration of dual solution are shown in Figure 3a,b for the variation in α and Γ_1 by fixing the values of $\Lambda_1 = 2$, $\Lambda_2 = -0.1$, $\phi = 0.1$, and $M = 1$. Figure 3a shows effect stretching case and obtained the dual solution by increasing the value of Γ_2 the limiting value of Γ_1 is decreases. Figure 3b shows the effect of the shrinking case dual solution, by increasing the value of Γ_2 the limiting value of Γ_1 is increased.

Figure 4a,b show the existence of a dual solution for the variation in $f_{\eta\eta}(0)$ and Γ_1 by fixing the values of $\Delta_1 = 2$, $\Lambda_2 = -0.1$, $\phi = 0.1$, and $M = 1$. Figure 4a shows the effect of stretching case the dual solution exist with $\Gamma_1 < -1$, and unique solution exists at $\Gamma_1 = -1$ and the magnitude of skin friction increases with decreasing value of Γ_1. Furthermore, it is observed that the upper branch solution increases with increasing Γ_2 but the behavior the lower branch solution is opposite. In Figure 4b, we show the effect of shrinking case and obtained the unique solution exists at $\Gamma_1 = -1$ and dual solution exist $\Gamma_1 > -1$, the magnitude of skin friction coefficients $f_{\eta\eta}(0)$ decreases with decreasing value of Γ_1. Furthermore, the dual branch solution is vanishing when Γ_1 reduces to -1.

Figure 5a–d depicts the variations $f(\eta)$ and $f_\eta(\eta)$ with the similarity η at the different value of the Γ_1 with the fixed value of $\Delta_1 = 2$, $\Lambda_2 = -0.1$, $\Gamma_2 = 2$, $\phi = 0.1$, and $M = 1$. The speed of the moving sheet is dependent on the value of Γ_1. The sheet moving speed is precisely cancelled by the mass-suction produced slip velocity at $\Gamma_1 = -1$, and it is found that the fluid flow vertically with a uniform velocity equal to v_w, when $\Gamma_1 > -1$ the upper branch solution's boundary layer thickness is smaller than that of the lower branch solution. In both the stretching and shrinking case the boundary layer thickness of the upper branch solution increases and decreases, respectively, by decreasing the value of Γ_1; the lower branch solutions behaves oppositely, when $\Gamma_1 < -1$. In both stretching and shrinking case

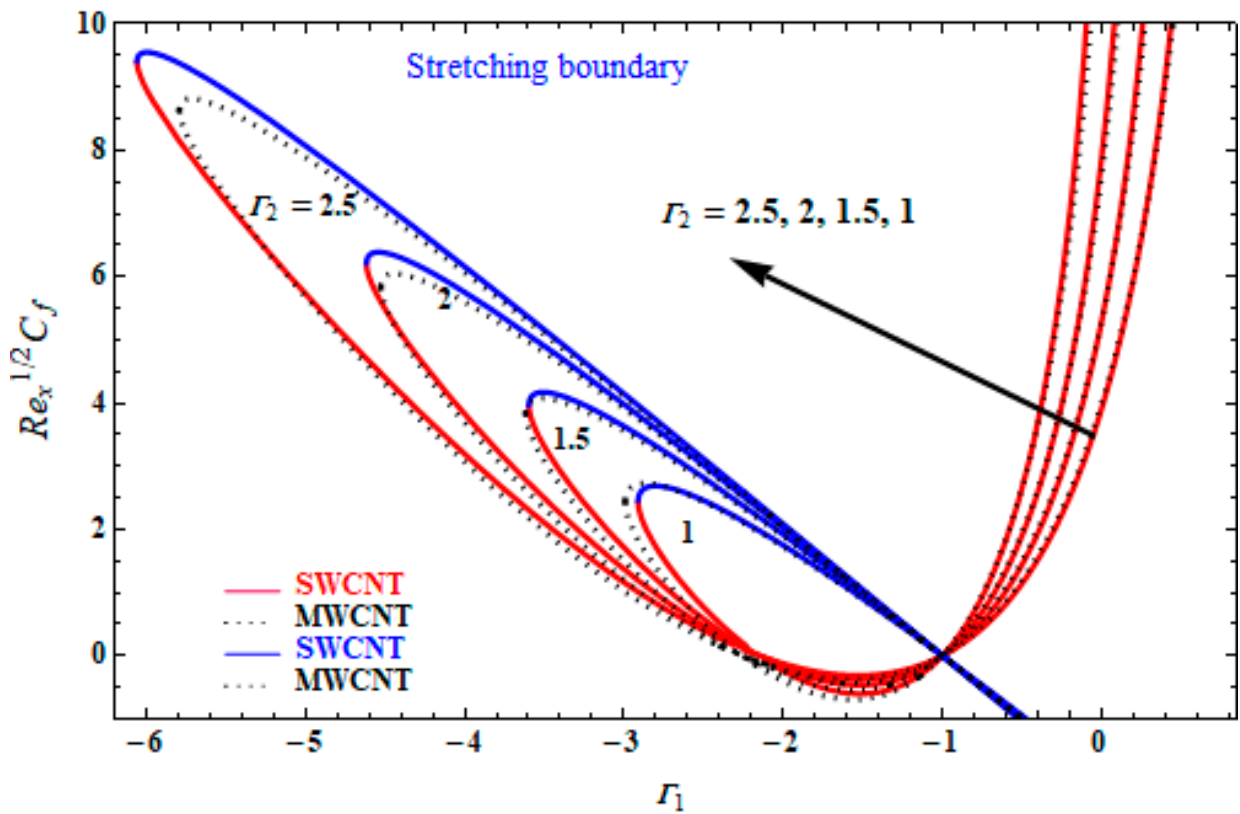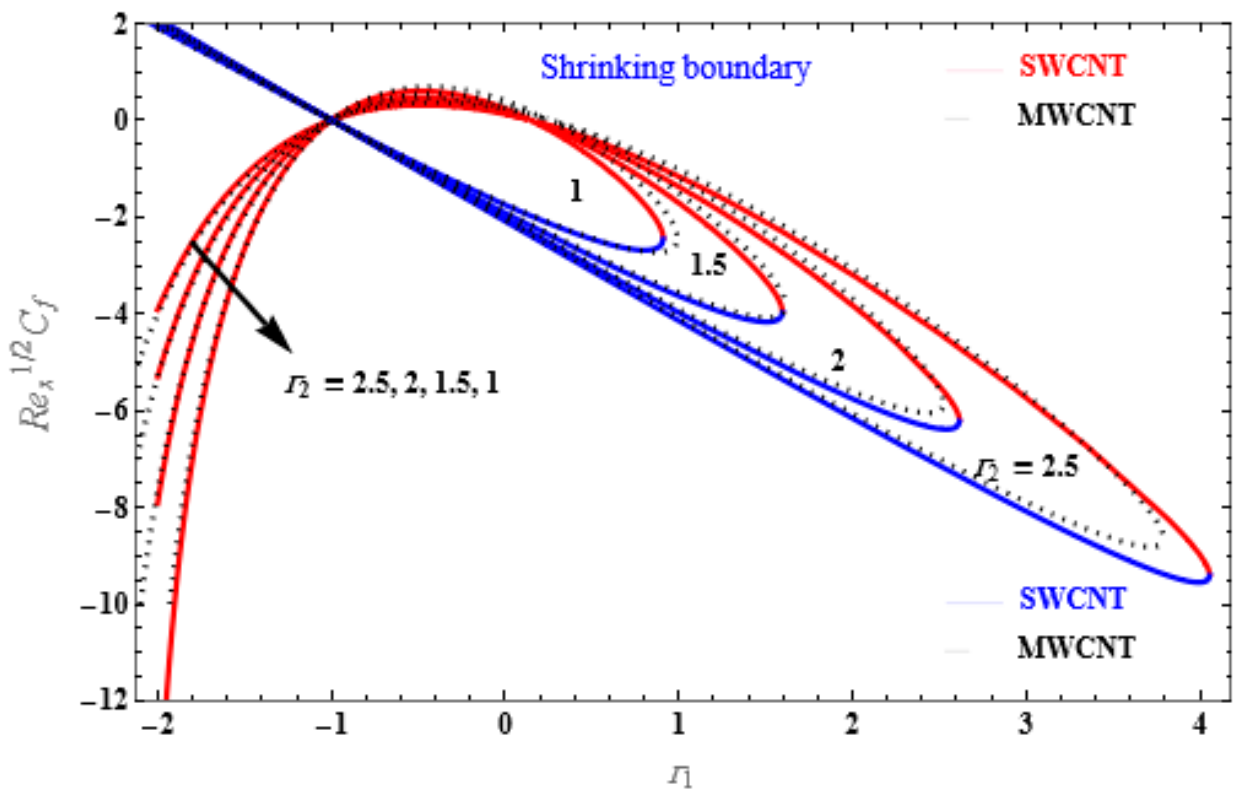the unique solution boundary layer thickness increases and decreases, respectively, with the decrease in Γ_1.
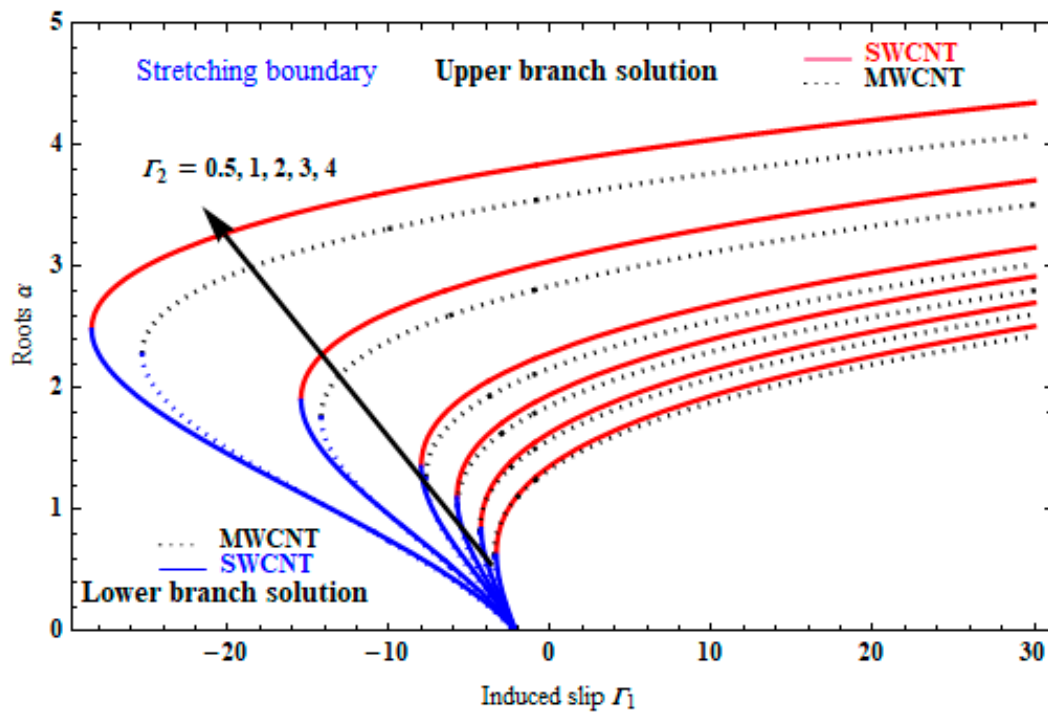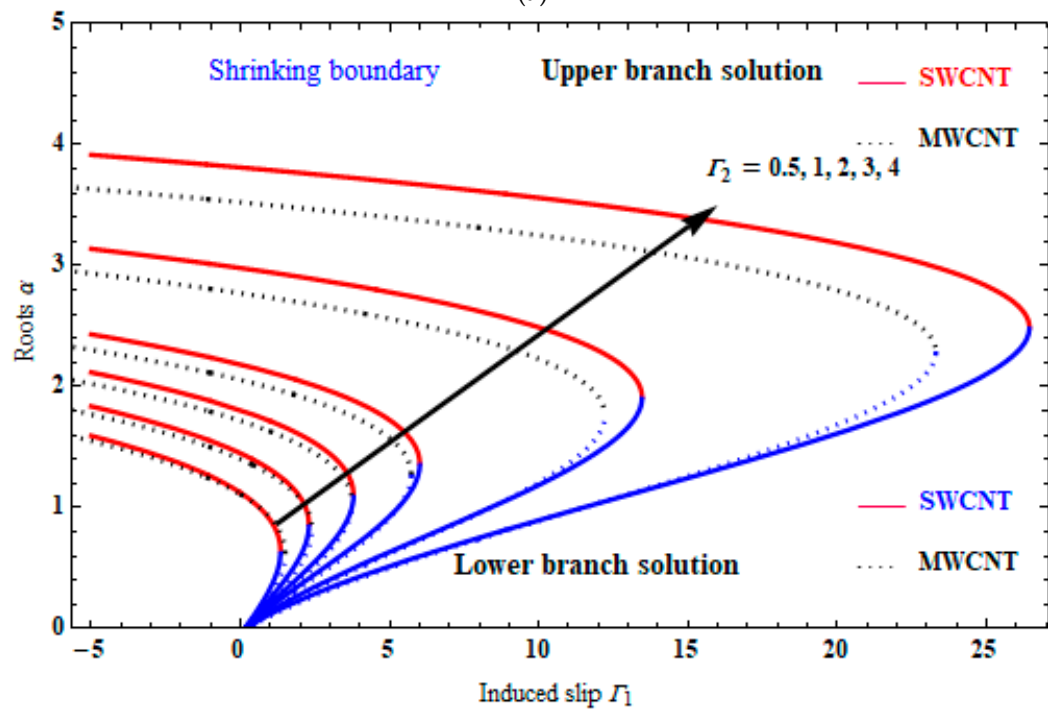
Figure 3. Plot of α versus Γ_1. (**a**) Stretching case; (**b**) shrinking case.

Figure 4. Plot $\mathrm{Re}_x^{1/2}C_f$ verses Γ_1, (**a**) stretching case (**b**) shrinking case.

Figure 5. *Cont.*

(c)

(d)
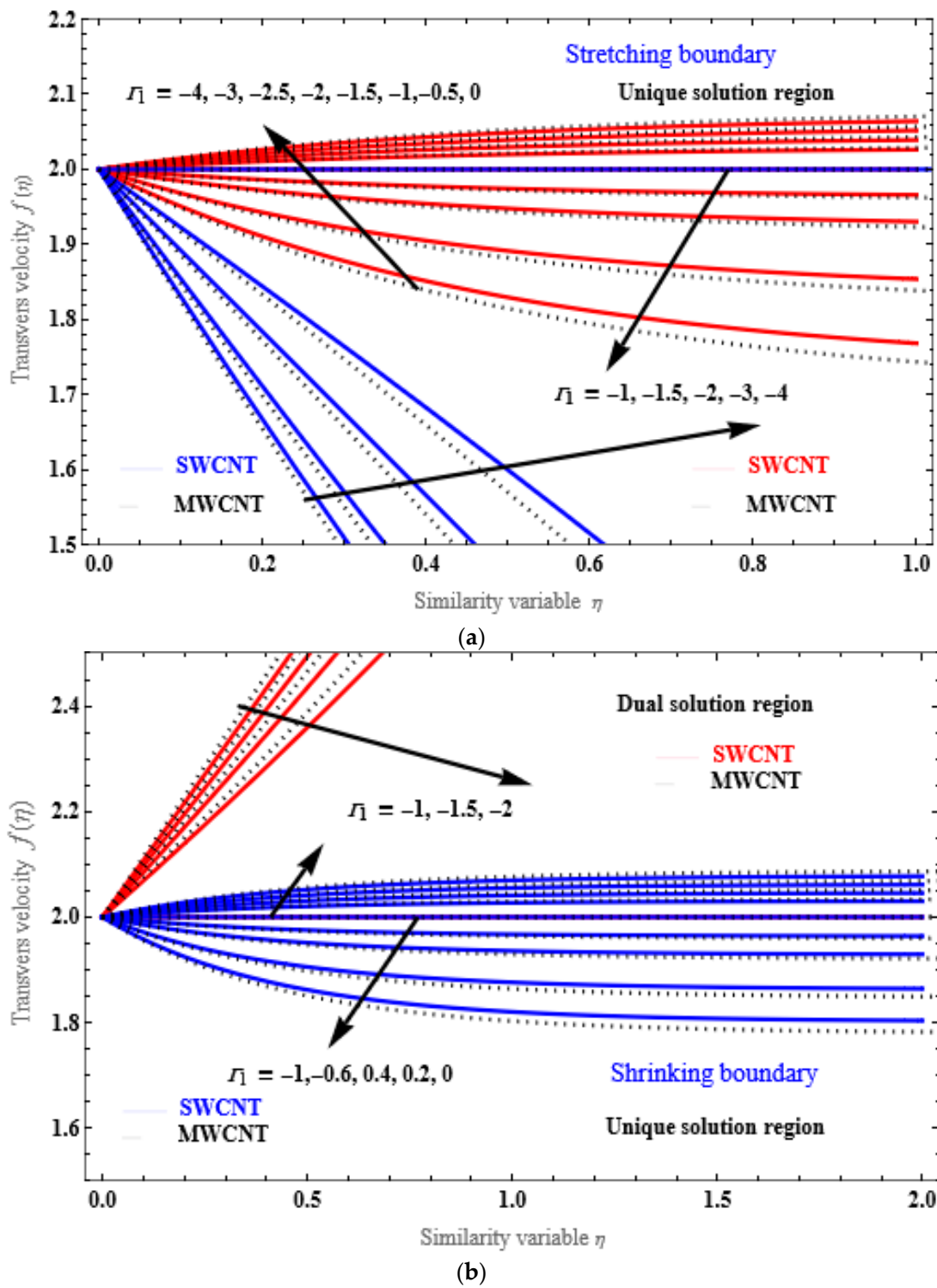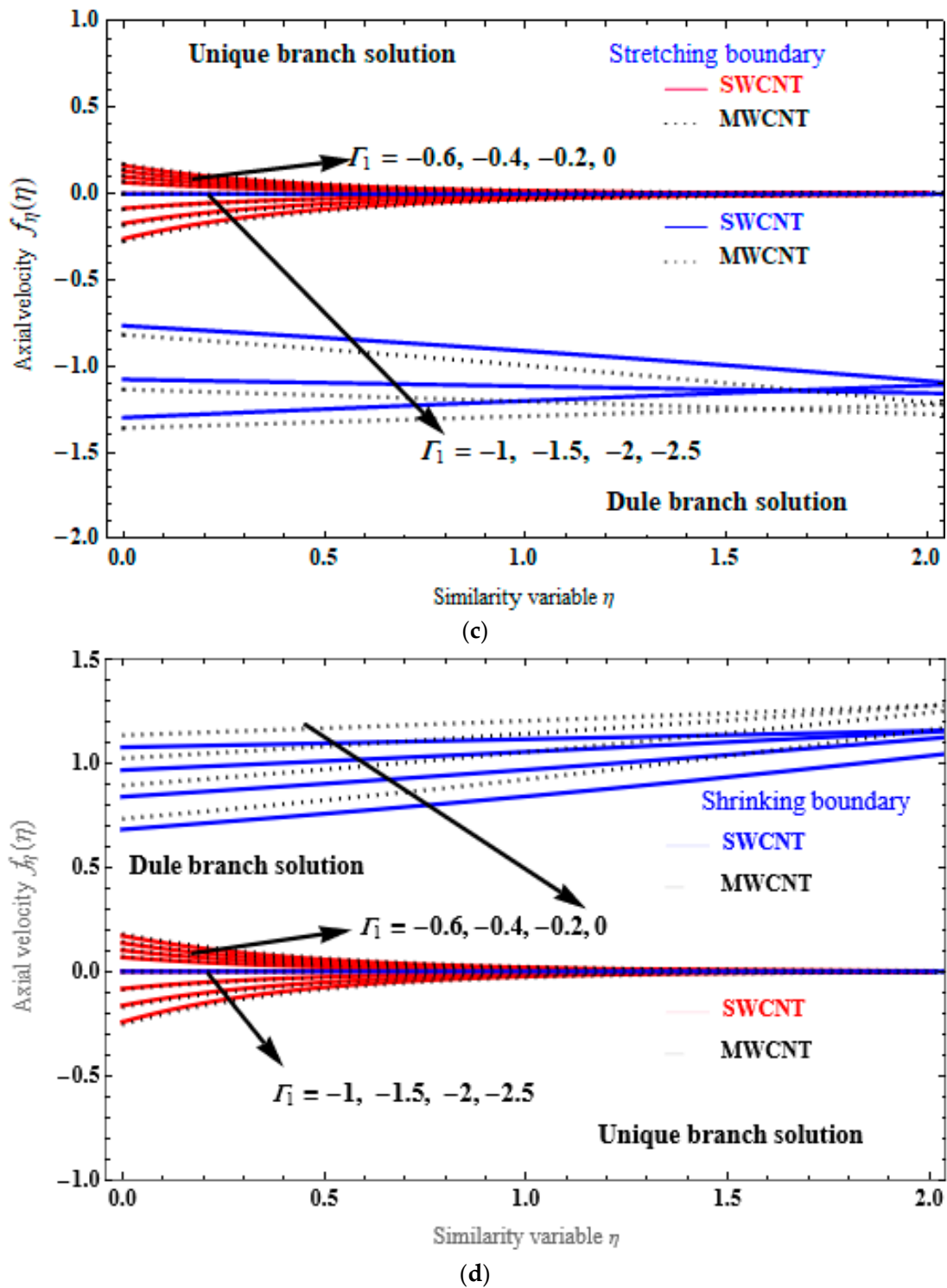
Figure 5. Plots of fluid velocity verses η with effect of Γ_1. (**a**) Transvers velocity (Stretching boundary), (**b**) Transvers velocity (Shrinking boundary), (**c**) Axial velocity (Stretching boundary) and (**d**) Axial velocity (Shrinking boundary).

Figure 6a,b show that there exists a unique solution for mass injection for the stretching case for the variation in α and Γ_1 by fixing the values of $\Lambda_1 = 2, \Lambda_2 = -0.1, \phi = 0.1$ and $M = 1$. Furthermore, it depicts that the solution α increases with the increasing value of Γ_1 and Γ_2. In this case MWCNT has more fluid flow compered with SWCNT.

(a)

(b)
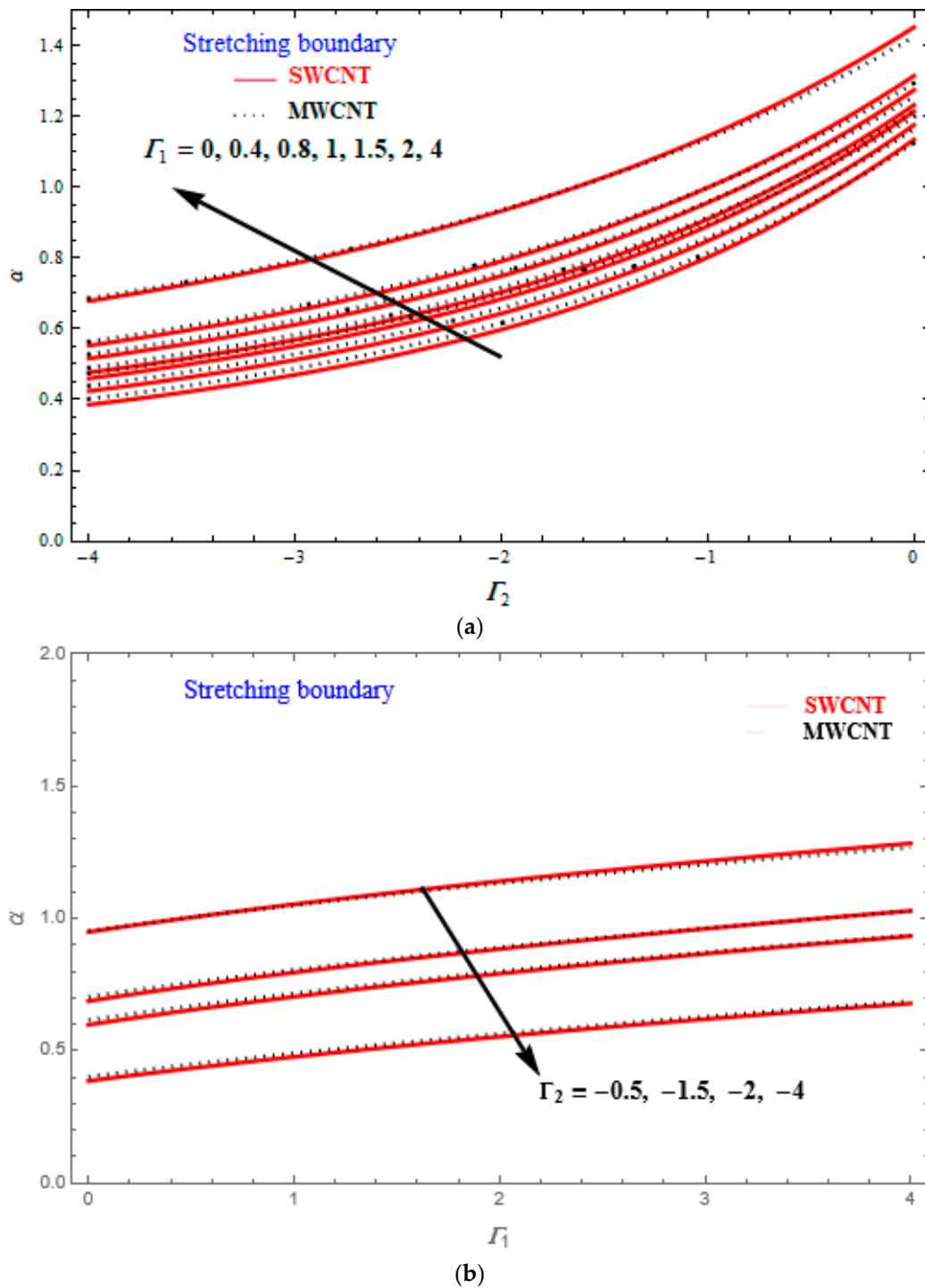
Figure 6. (**a**) Plot α verses Γ_2, and (**b**). (**a**) Plot α verses Γ_1, on stretching case.

Figure 7a,b depict transvers and axial velocity profile with the variation in similarity η at the different value of the Γ_1 for the stretching and shrinking case with the fixed value, for the stretching case of $\Delta_1 = 2, \Lambda_2 = -0.1, \Gamma_2 = -2, \phi = 0.1, M = 1$ and for the shrinking case $\Delta_1 = 2, \Lambda_2 = -0.1, \Gamma_2 = -2, \phi = 0.1, M = 2$. It is found that the thickness of the boundary layer reduces as Γ_1 increases in Figure 7a,b, whereby the fluid flow in SWCNT and MWCNT has a positive vertical velocity that is gradually decreasing (become negative) as one moves far enough away from the sheet. Further, fluid flow in the SWCNT decreases faster than the MWCNT.
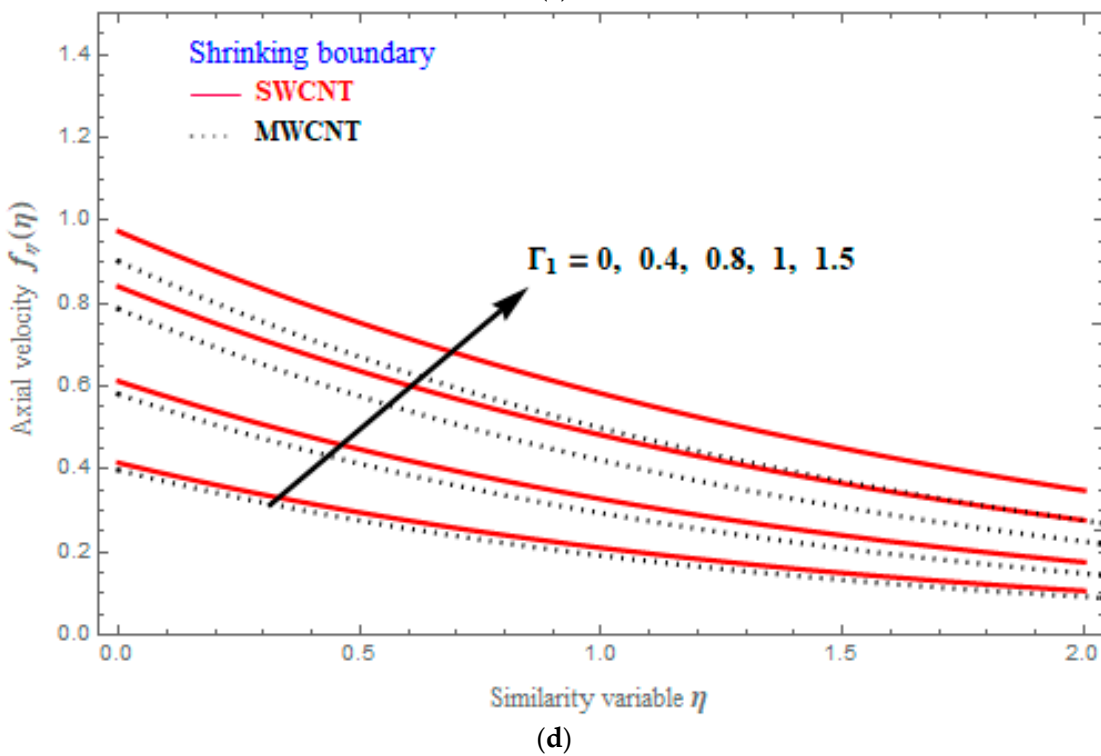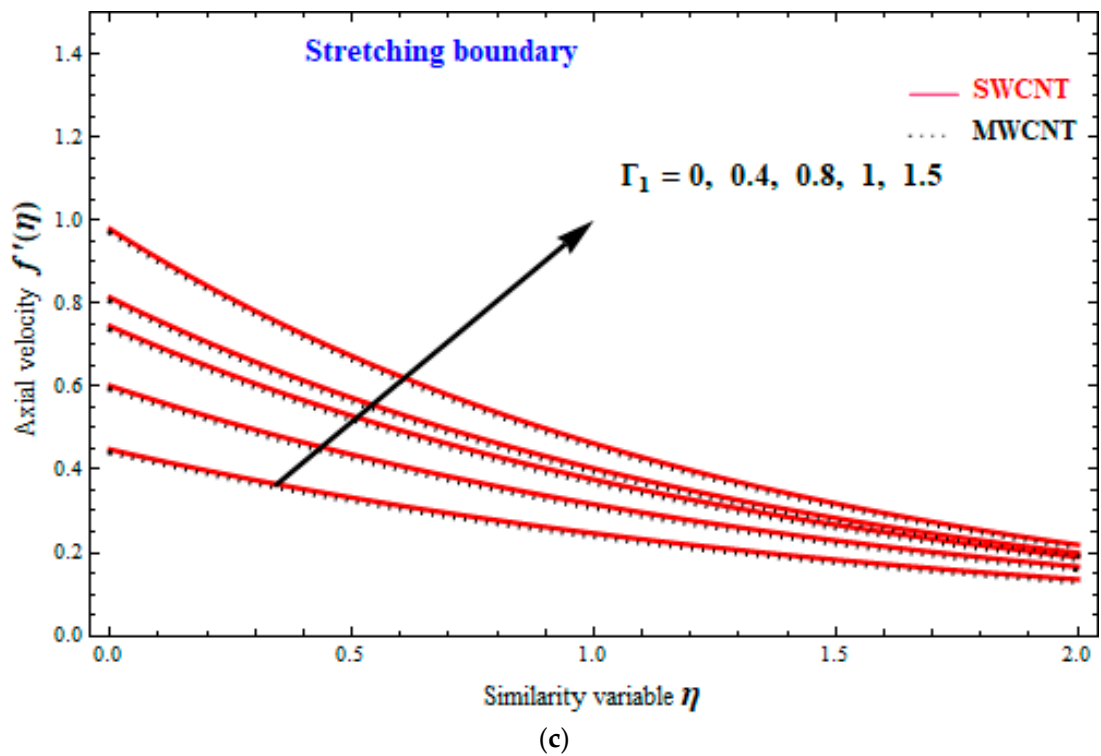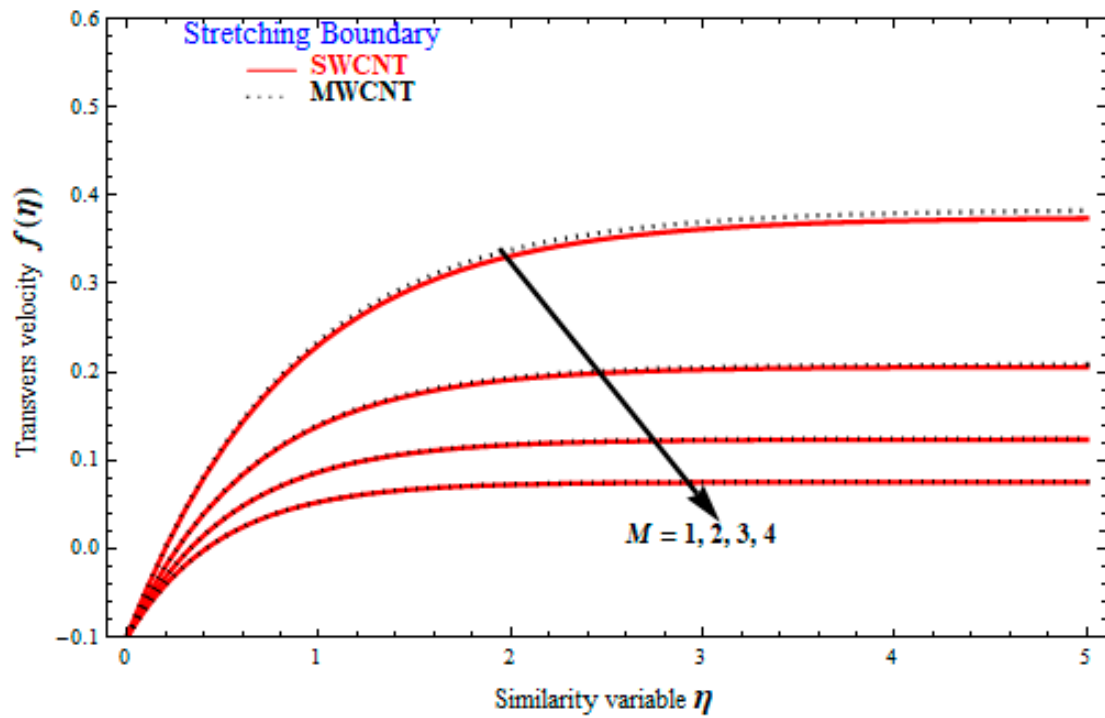
Figure 7. *Cont.*
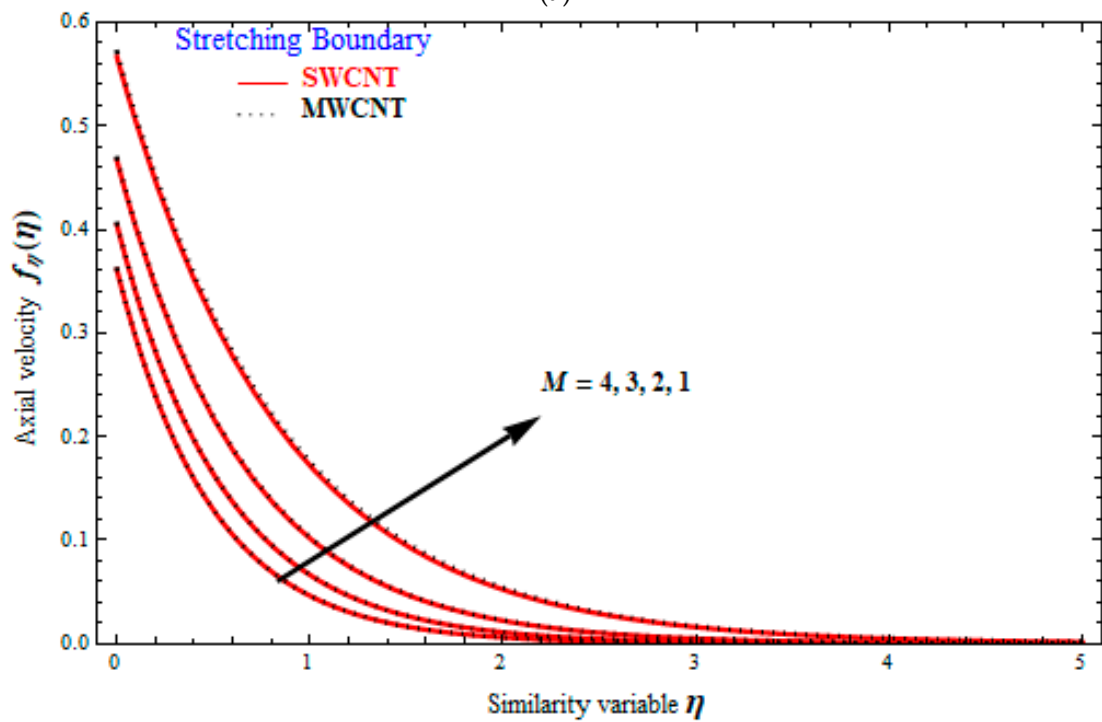
(c)

(d)
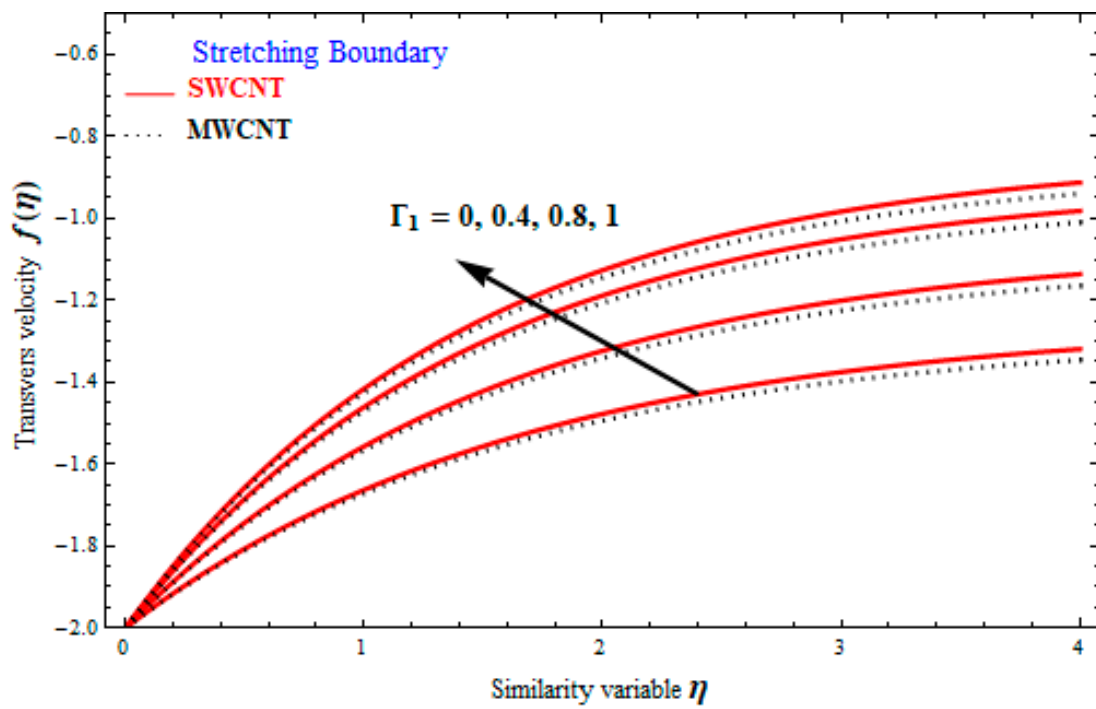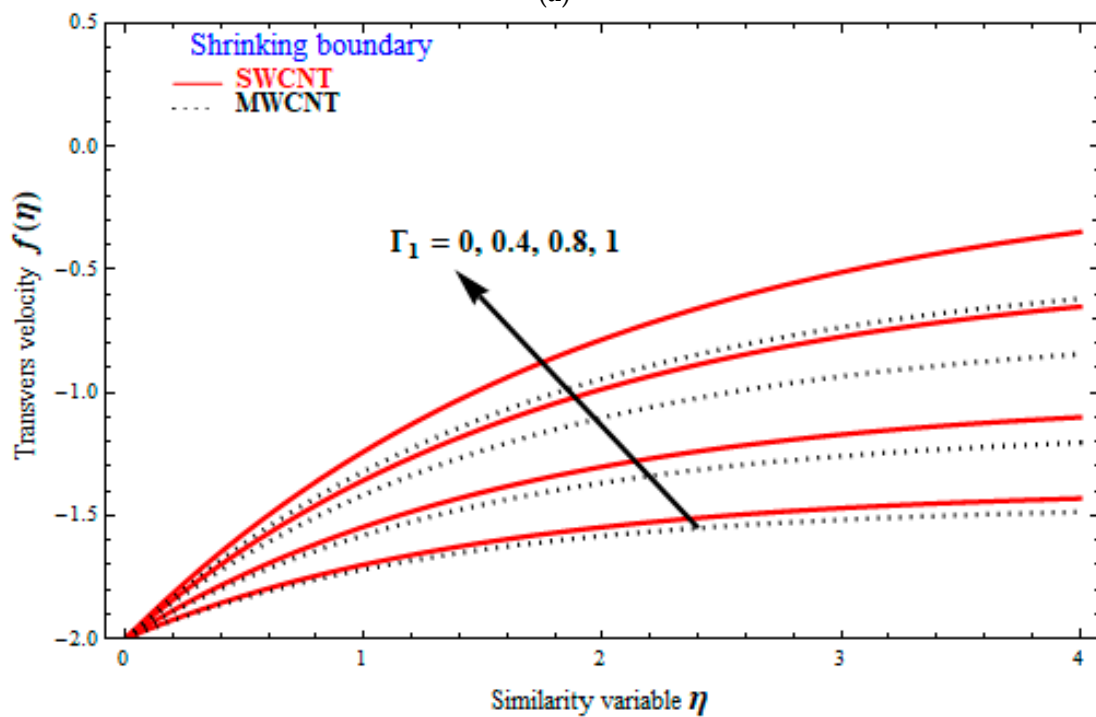
Figure 7. Plot of $f(\eta)$ and $f_\eta(\eta)$ with similarity variable η with effect of Γ_1. (**a,c**) Stretching case, (**b,d**) shrinking case.

Figure 8a,b depict transvers and axial velocity profile with the variation in similarity η at the different value of the M for both stretching and shrinking case. For the Figure 7a–d the value of $\Delta_1 = 2, \Lambda_2 = -0.1, \Gamma_2 = -0.1, \Gamma_1 = 1, \phi = 0.1$, are fixed and it is noted that the boundary layer thickness is decreases with increasing the magnetic field M.
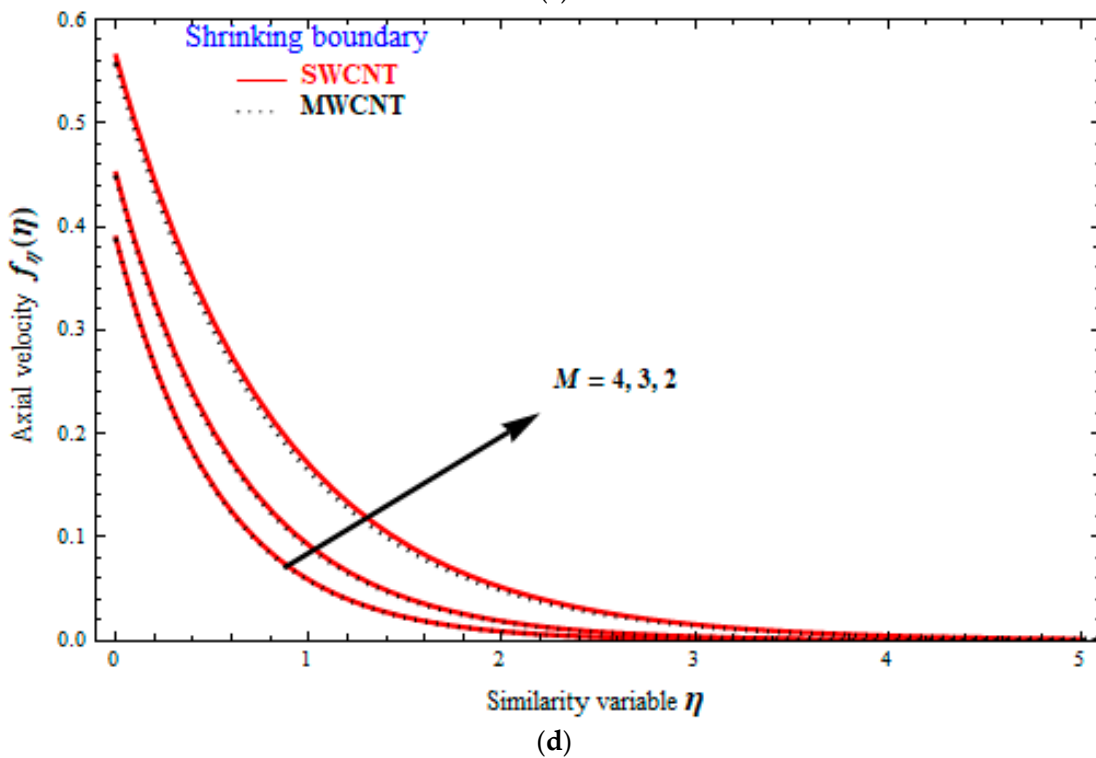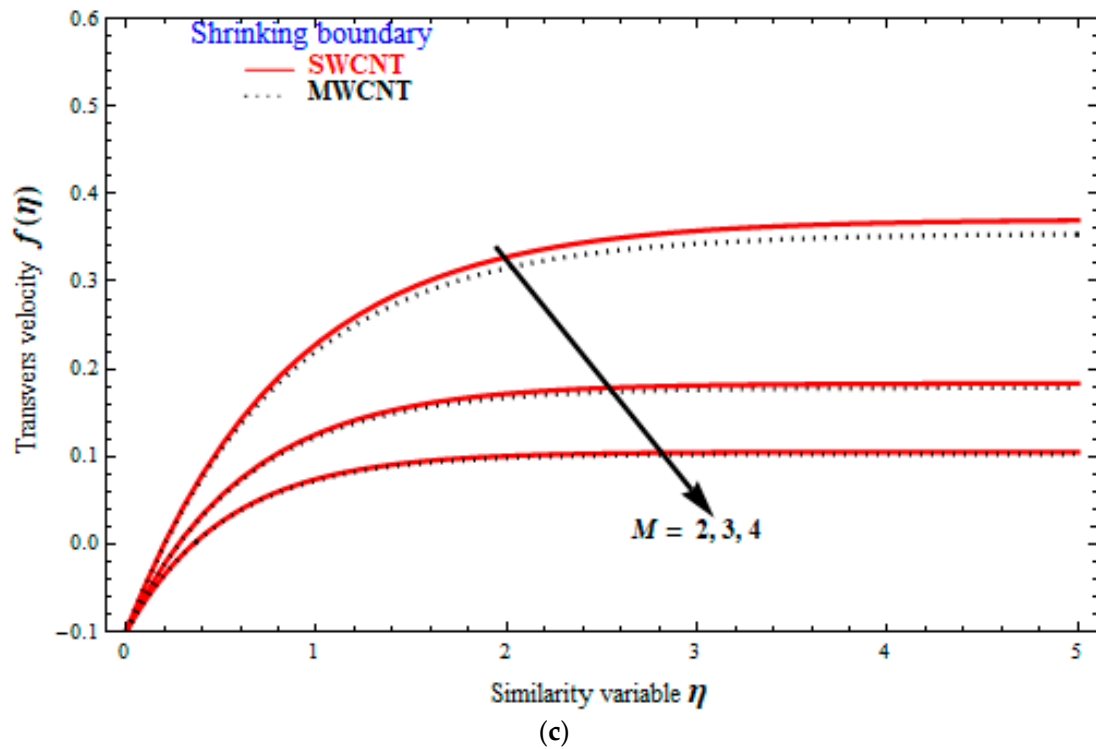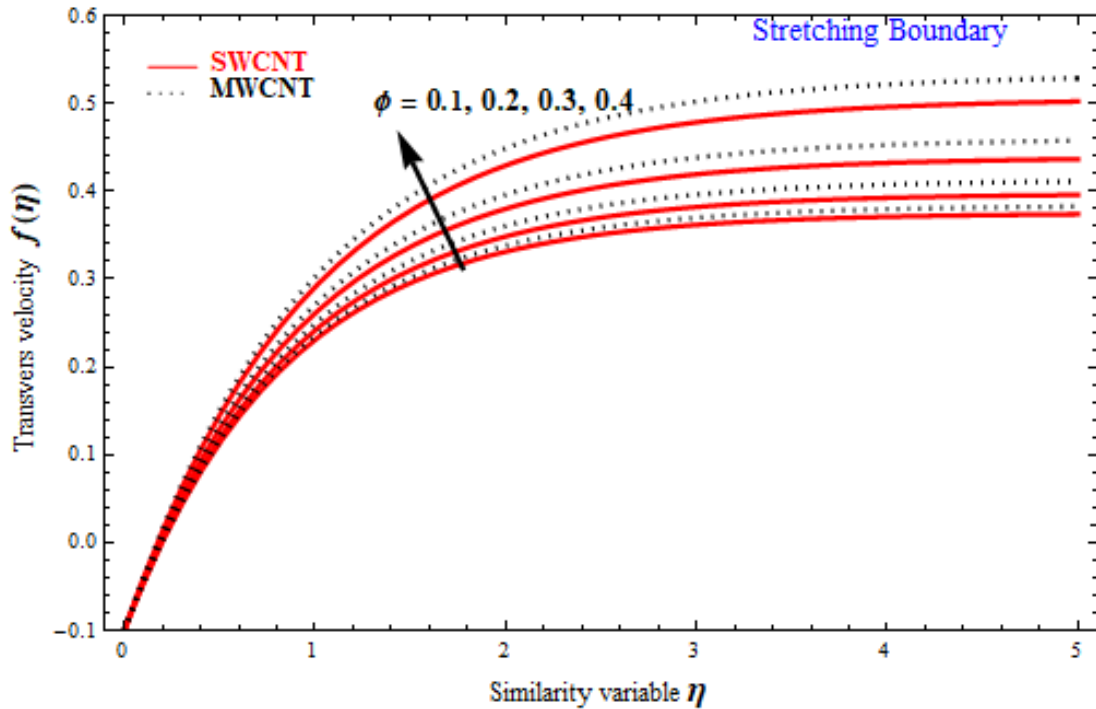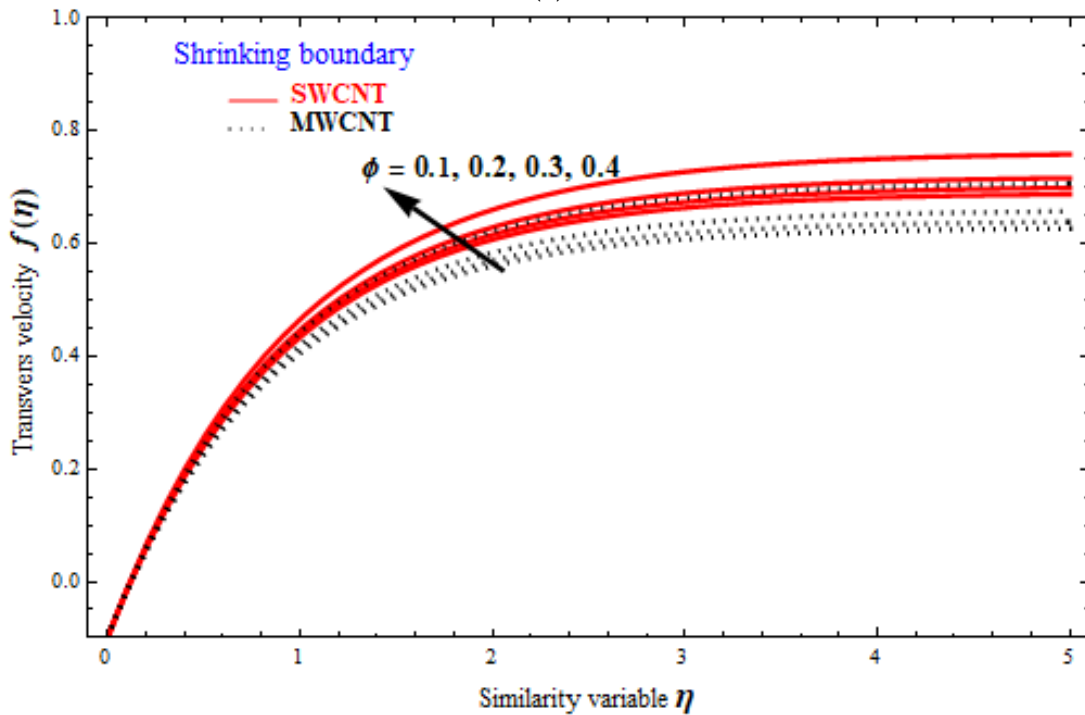
Figure 8. *Cont*.

(c)

(d)

Figure 8. Plot of $f(\eta)$ and $f_\eta(\eta)$ with similarity variable η with effect of M. (**a**,**b**) Stretching case, (**c**,**d**) shrinking case.

Figure 9a,b depict transvers and axial velocity profile with the variation in similarity η at the different value of the ϕ for both stretching and shrinking case. For the Figure 9a,b the value of $\Delta_1 = 2$, $\Lambda_2 = -0.1$, $\Gamma_2 = -0.1$, $\Gamma_1 = 1$, $M = 1$, and Figure 9c,d $\Delta_1 = 2$, $\Lambda_2 = -0.1$, $\Gamma_2 = -0.1$, $\Gamma_1 = 1$, $M = 2$, are fixed and it is noted that the boundary layer thickness is increased with increasing the solid volume fraction ϕ. The effects of magnetic field (M), the solid volume fraction (ϕ), thermal radiation (N_r), are demonstrated in Figure 10a–f

on the temperature profile for both stretching and shrinking case. The value of physical parameters are fixed as follows Figure 10a,b $\Delta_1 = 2$, $\Lambda_2 = -0.1$, $\Gamma_2 = -0.1$, $\phi = 0.1$, $\Gamma_1 = 1$, $Pr = 6.2$, $Nr = 1$, and Figure 10c $\Delta_1 = 2$, $\Lambda_2 = -0.1$, $\Gamma_2 = -0.1$, $Nr = 1$, $\Gamma_1 = 1$, $M = 1$, $Pr = 6.2$, Figure 10d $\Delta_1 = 2$, $\Lambda_2 = -0.1$, $\Gamma_2 = -0.1$, $Nr = 1$, $\Gamma_1 = 1$, $M = 2$, $Pr = 6.2$, Figure 10e $\Delta_1 = 2$, $\Lambda_2 = -0.1$, $\Gamma_2 = -0.1$, $\phi = 0.1$, $\Gamma_1 = 1$, $M = 1$, $Pr = 6.2$, Figure 10f $\Delta_1 = 2$, $\Lambda_2 = -0.1$, $\Gamma_2 = -0.1$, $\phi = 0.1$, $\Gamma_1 = 1$, $M = 2$, $Pr = 6.2$,
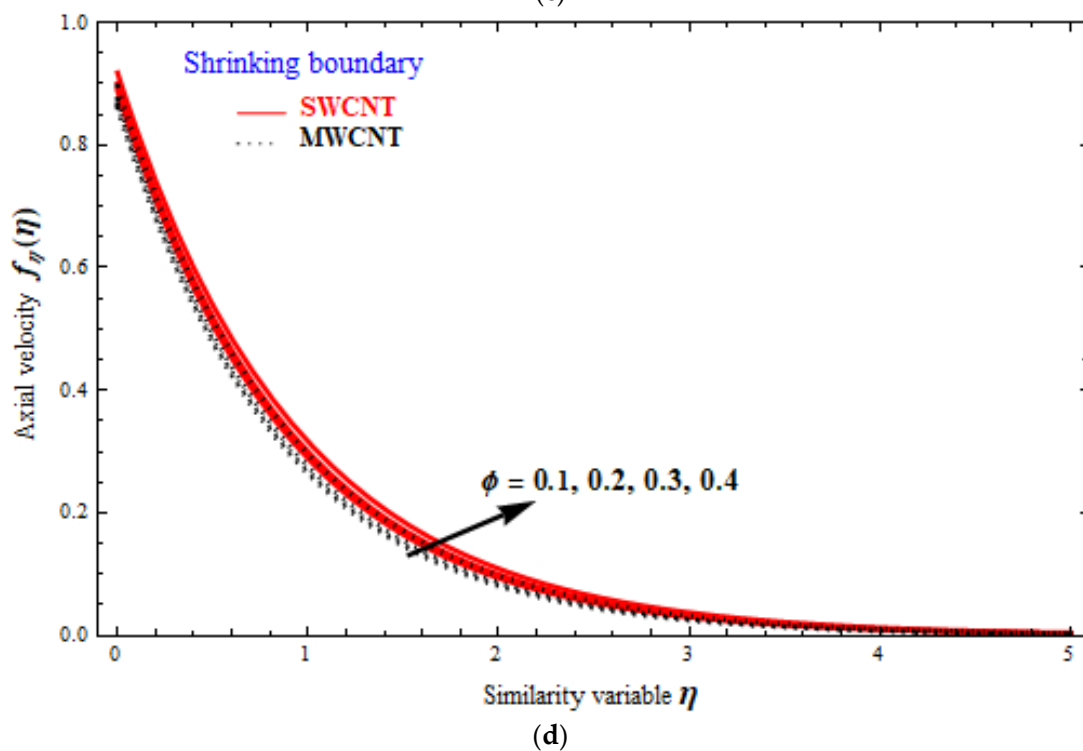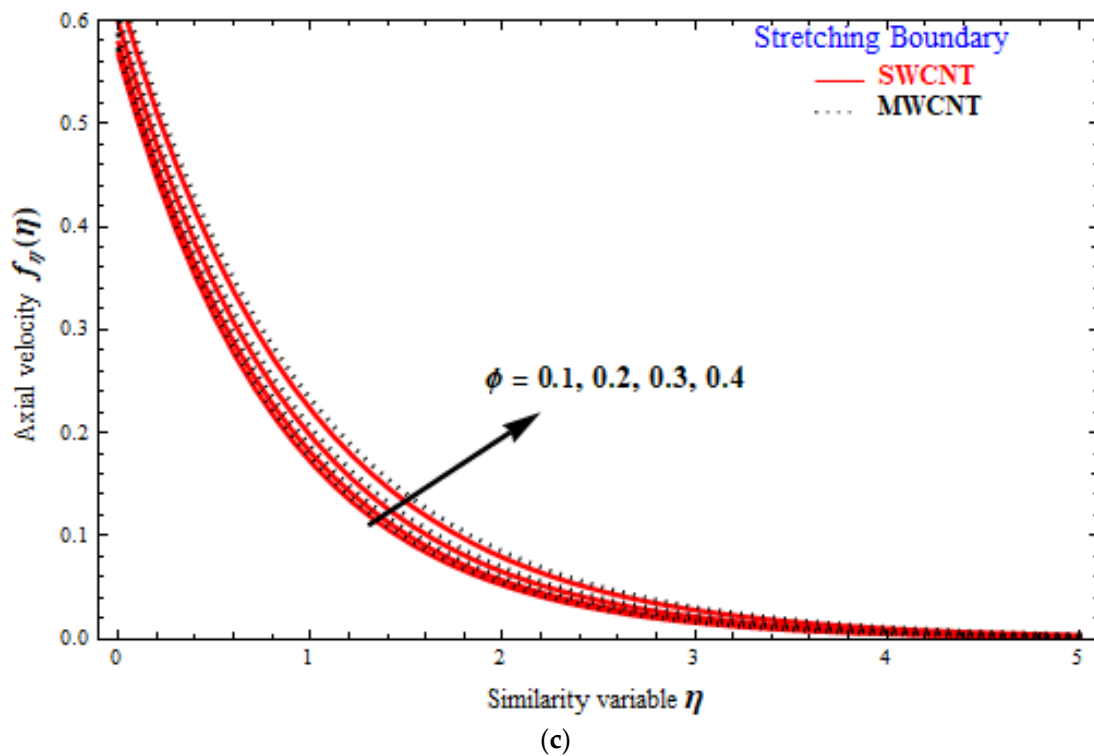

(a)

(b)

Figure 9. *Cont.*

(c)

(d)

Figure 9. Plot of $f(\eta)$ and $f_\eta(\eta)$ with similarity variable η with effect of ϕ. (**a,b**) Stretching case, (**c,d**) shrinking case.

- In Figure 10a,b the thermal boundary layer thickness of SWCNT and MWCNT is increased with increasing the magnetic field M. Further, it is observed that SWCNT has more energy compeer to the MWCNT for both stretching and shrinking cases;
- By increasing the solid volume fraction, the thermal boundary layer thickness of SWCNT and MWCNT increases in both cases. Furthermore, it is observed that 10c

SWCNT have more heat energy compered with MWCNT, and in Figure 10d SWCNT and MWCNT have some energy;

- The increasing values of N_r result in greater thickness in thermal boundary as show in Figure 10e,f. Further, it is observed that SWCNT have more thermal energy compered with MWCNT.
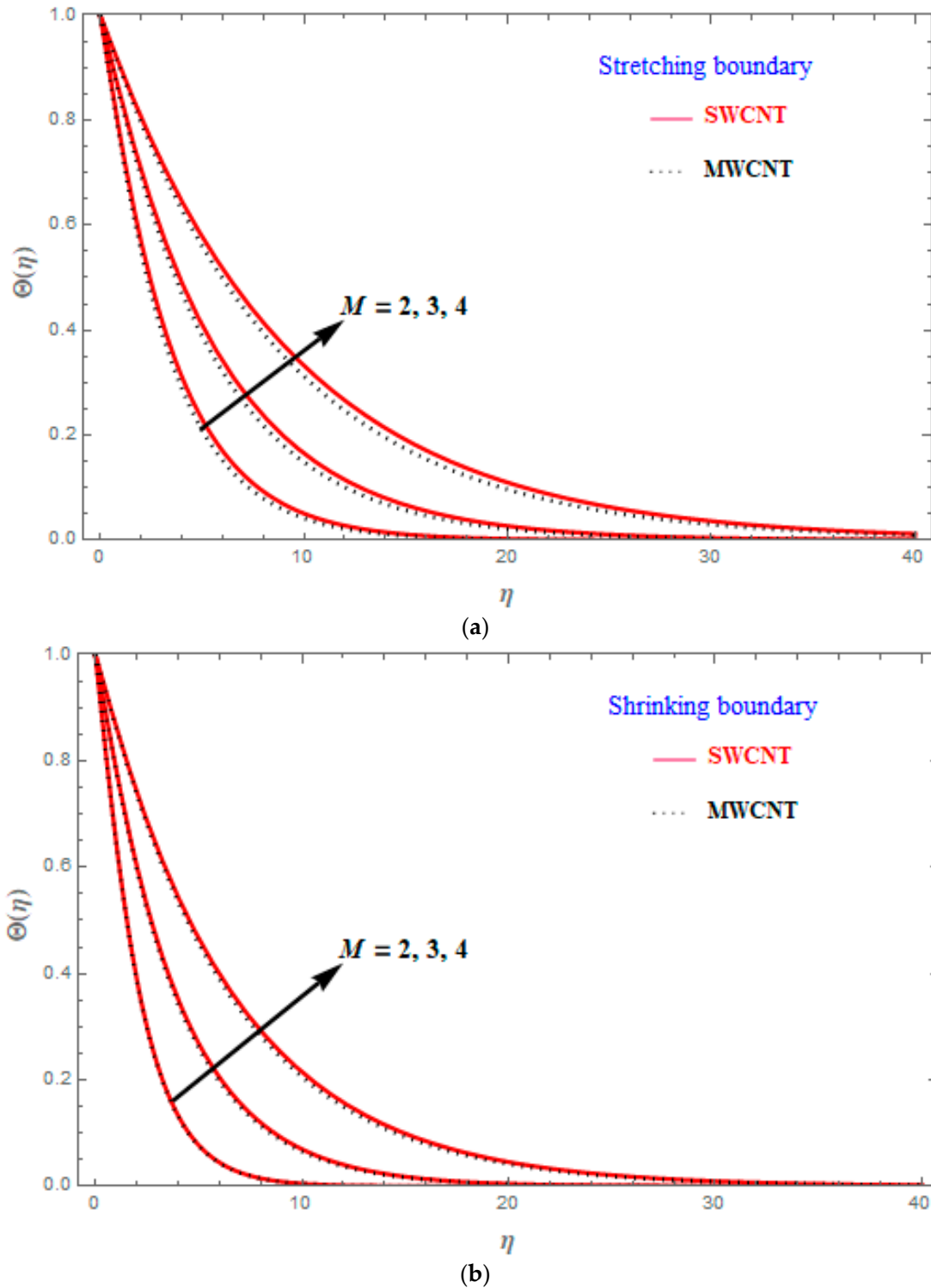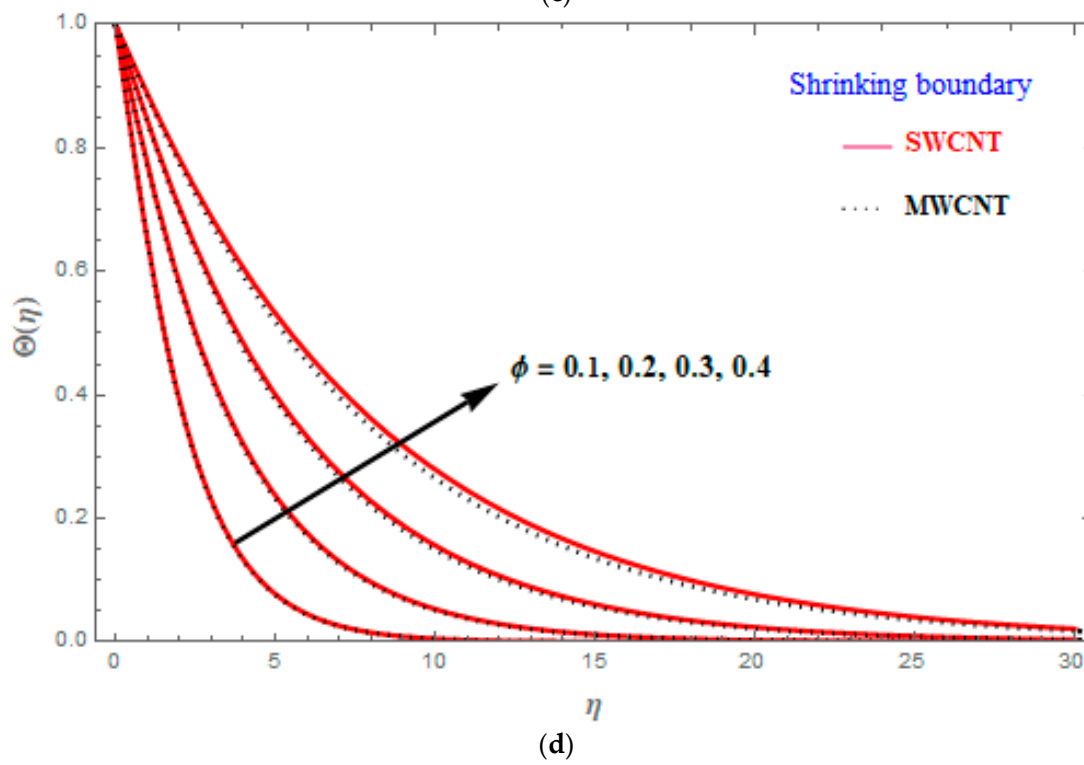

(a)

(b)

Figure 10. *Cont.*

(**c**)

(**d**)

Figure 10. *Cont.*

(e)

(f)
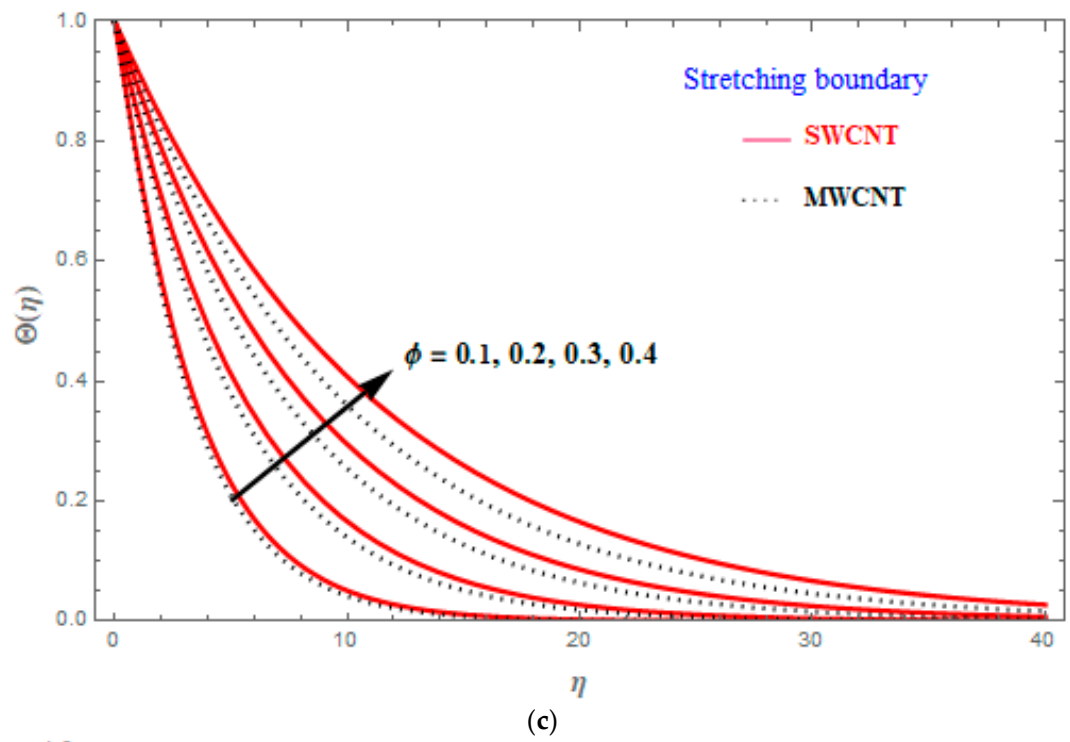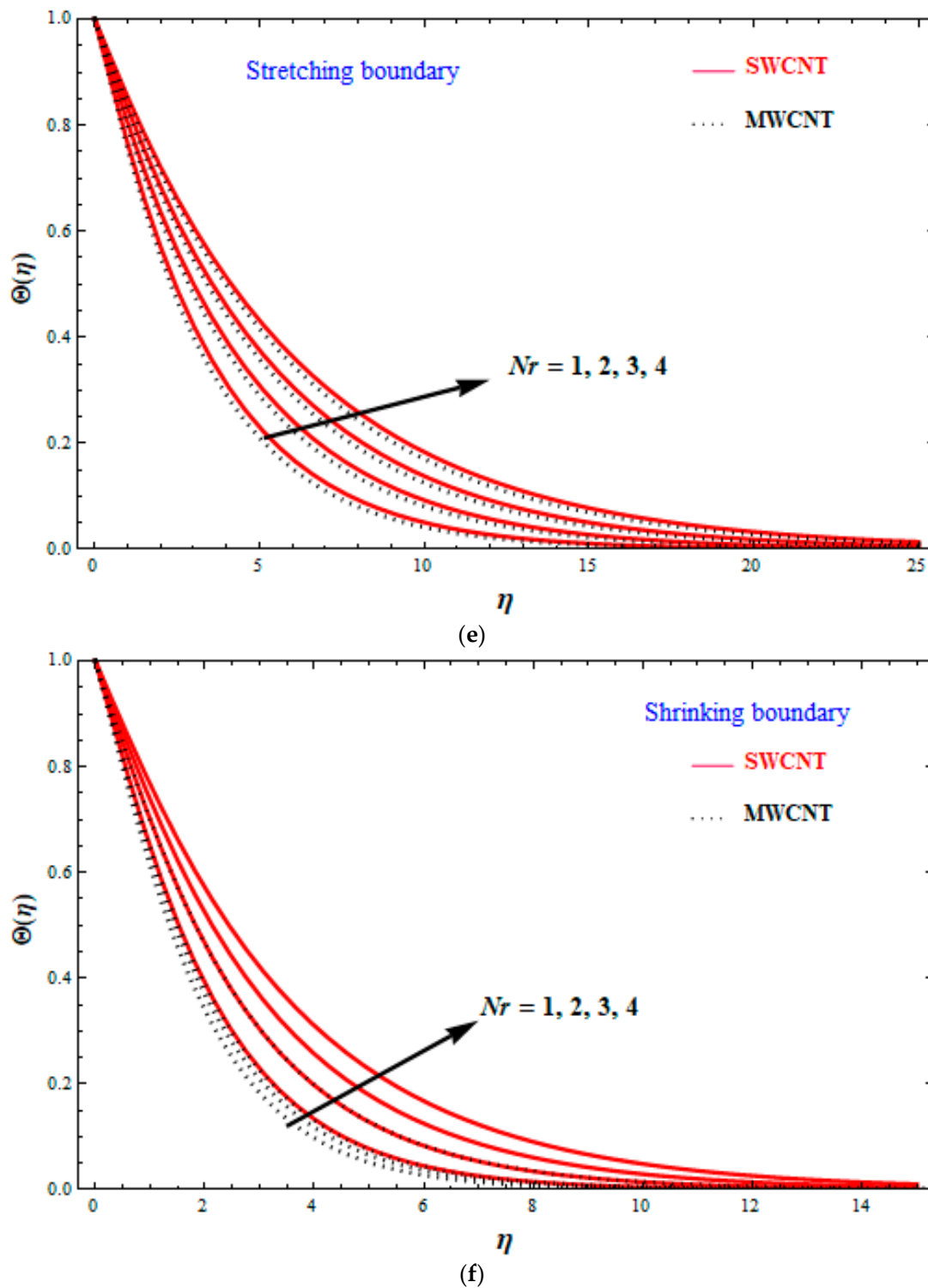
Figure 10. (**a–f**) plot of $\Theta(\eta)$ with similarity variable η with effect (**a**) M on stretching case, (**b**) M on shrinking case, (**c**) ϕ on stretching case, (**d**) ϕ on shrinking case, (**e**) Nr on stretching case, (**f**) Nr on shrinking case.

4. Summary and Conclusions

The present paper investigates the analytical solution of fluid flow of the stretching/shrinking sheet in the prances of the carbon nanotubes with induced slip on heat transfer of inclined magnetic field and radiation with mass transpiration. The following conclusions were obtained in this study:

- In the absence of CNTs and inclined magnetic field the results are similar to those presented in previous references [20,21];
- When fluid is injected into the SWCNT and MWCNT the flow of the fluid is along the direction of the motion of the surface and in the suction case the direction of the flow is changed due to the prances of mass transfer-induced slip, which has an impact on the convection process that transfers heat;
- For both stretching and shrinking cases, the impact of induced slip with mass suction significantly extend the unique and dual solution region of SWCNT and MWCNT;
- In the presence of the mass-injection slip, the velocity of fluid in SWCNT and MWCNT is increased which increases the speed of the flow along the sheet;
- By increasing the value of the Γ_1 and ϕ, both transverse and axial velocity increases both cases of stretching and shrinking;
- By increasing the value of the M the transverse velocity decreases and axial velocity increases both cases of stretching and shrinking;
- The thermal boundary layer thickness is increased while increasing physical parameters such as radiation (N_r), volume fraction, (ϕ) and magnetic field (M) for both cases of stretching and shrinking.

Finally, let us comment that in this research we showed that the fluid flow in SWCNT has higher temperature than MWCNT by using the induced slip condition with the combination of inclined MHD and CNTs. Table 2 lists the thermophysical properties of the nanofluids. For the velocity behavior in the absences of CNTs and inclined MHD, the results are reduced to Wu's results [23]. Moreover, the results provided in ref. [24] in absence of thermal radiation are recovered too. In Table 3 a comparison with previous results is presented.

Table 2. Variation in thermophysical properties of nanofluids with solid volume fraction of CNTs.

SWCNT	ϕ	μ_{nf}	ρ_{nf}	$(\rho C p)_{nf}$	κ_{nf}	σ_{nf}
	0.1	1.30135	1.16076	0.926519	2.90881	1.33333
	0.2	1.74695	1.32151	0.853037	5.29387	1.75000
	0.3	2.43924	1.48227	0.779556	0.35882	2.28571
MWCNT						
	0.1	1.30135	1.06047	0.926517	2.73334	1.33333
	0.2	1.74693	1.12093	0.853037	4.89830	1.75000
	0.3	2.43924	1.8114	0.779556	7.67900	2.28571

Table 3. Comparative analysis on governing equation provided in the literature.

Authors	Fluids	The Governing Equation
Wu [23]	Newtonian	$u\dfrac{\partial u}{\partial x} + v\dfrac{\partial u}{\partial y} = -\dfrac{1}{\rho}\dfrac{\partial p}{\partial x} + v_{nf}\left[\dfrac{\partial^2 u}{\partial x^2} + \dfrac{\partial^2 u}{\partial y^2}\right],$ $u\dfrac{\partial v}{\partial x} + v\dfrac{\partial v}{\partial y} = -\dfrac{1}{\rho}\dfrac{\partial p}{\partial x} + v_{nf}\left[\dfrac{\partial^2 v}{\partial x^2} + \dfrac{\partial^2 v}{\partial y^2}\right],$
Wu [24]	Newtonian	$u\dfrac{\partial T}{\partial x} + v\dfrac{\partial T}{\partial y} = \alpha_{nf}\dfrac{\partial^2 T}{\partial y^2},$
Present work	Newtonian	$u\dfrac{\partial u}{\partial x} + v\dfrac{\partial u}{\partial y} = -\dfrac{1}{\rho}\dfrac{\partial p}{\partial x} + v_{nf}\left[\dfrac{\partial^2 u}{\partial x^2} + \dfrac{\partial^2 u}{\partial y^2}\right] - \dfrac{\sigma_{nf} B_0{}^2}{\rho_{nf}}\sin^2(\tau)u,$ $u\dfrac{\partial v}{\partial x} + v\dfrac{\partial v}{\partial y} = -\dfrac{1}{\rho}\dfrac{\partial p}{\partial x} + v_{nf}\left[\dfrac{\partial^2 v}{\partial x^2} + \dfrac{\partial^2 v}{\partial y^2}\right] - \dfrac{\sigma_{nf} B_0{}^2}{\rho_{nf}}\sin^2(\tau)v,$ $u\dfrac{\partial T}{\partial x} + v\dfrac{\partial T}{\partial y} = \alpha_{nf}\dfrac{\partial^2 T}{\partial y^2} - \dfrac{1}{(\rho C p)_{nf}}\dfrac{\partial q_r}{\partial y}.$

Nomenclature

This appendix declares the different symbols used in the text of the manuscript and their corresponding SI units (if relevant).

Symbol	Explanations	S.I Unit
Latin symbols		
A_1, A_2, A_3, A_4, A_5	Constant	$[-]$
B_0	Applied magnetic field	$[\text{wm}^{-2}]$
C_P	Specific heat at constant pressure	$[\text{JKg}^{-1}\text{K}^{-1}]$
k^*	Mean absorption coefficient	$[\text{m}^{-2}]$
M	Magnetic field	$[-]$
N_r	Radiation parameter	$[-]$
Pr	Prandtl number	$[-]$
q_r	Radiative heat flux	$[\text{Wm}^{-2}]$
q_w	Local heat flux at the wall	$[-]$
T	Temperature	$[\text{K}]$
V_c	Mass transformation	$[-]$
(x, y)	Co-ordinate axes	$[\text{m}]$
(u, v)	Velocities along *x*- and *y*- directions	$[\text{ms}^{-1}]$
Greek symbols		
κ	Thermal conductivity of fluid	$[\text{WKg}^{-1}\text{K}^{-1}]$
η	Similarity variable	$[-]$
μ_f	Dynamic viscosity of fluid	$[-]$
ν	Kinematic viscosity	$[-]$
ρ	Density	$[\text{Kgm}^{-3}]$
σ^*	Stefan–Boltzmann constant	$[-]$
Γ	Gamma function	$[-]$
ϕ	Nanoparticle volume fraction	$[-]$
ψ	Stream function	$[-]$
τ	Angle of inclination of magnetic field	$[-]$
Subscripts		
f	Base fluid	$[-]$
nf	Nanofluid	$[-]$
Abbreviations		
MHD	Magnetohydrodynamics	$[-]$
CNT	Carbon nanotubes	$[-]$
HNF	Hybrid nanofluid	$[-]$
SWCNT	Signal wall carbon nanotube	$[-]$
MWCNT	Multi-wall carbon nanotubes	$[-]$

Appendix A. Roots of the Fourth Order Polynomials

This appendix provides the explicit expressions for the roots of the fourth order polynomials:

$$\begin{cases}
\begin{cases}
\alpha_{1,2} = -\dfrac{q}{4p} - \dfrac{1}{2}\sqrt{\dfrac{q^2}{(4p^2)} - \dfrac{(2r)}{(3p)} + \dfrac{e}{g} + \dfrac{g}{3\times 2^{(1/3)}p} - \left(\dfrac{e}{g} + \dfrac{g}{3\times 2^{(1/3)}p}\right)} \\[4mm]
\dfrac{1}{2}\sqrt{\dfrac{q^2}{(2p^2)} - \dfrac{(4r)}{(3p)} - \dfrac{e}{g} + \dfrac{g}{3\times 2^{(1/3)}p} - \left(\dfrac{e}{g} + \dfrac{g}{3\times 2^{(1/3)}p}\right)} - \dfrac{-\frac{q^3}{p^3} + \frac{4qr}{p^2} - \frac{8s}{p}}{4\sqrt{\dfrac{q^2}{(4p^2)} - \dfrac{(2r)}{(3p)} + \dfrac{e}{g} + \dfrac{g}{3\times 2^{(1/3)}p} - \left(\dfrac{e}{g} + \dfrac{g}{3\times 2^{(1/3)}p}\right)}}
\end{cases} \\[12mm]
\begin{cases}
\alpha_{3,4} = -\dfrac{q}{4p} + \dfrac{1}{2}\sqrt{\dfrac{q^2}{(4p^2)} - \dfrac{(2r)}{(3p)} + \dfrac{e}{g} + \dfrac{g}{3\times 2^{(1/3)}p} - \left(\dfrac{e}{g} + \dfrac{g}{3\times 2^{(1/3)}p}\right)} \\[4mm]
\pm\dfrac{1}{2}\sqrt{\dfrac{q^2}{(2p^2)} - \dfrac{(4r)}{(3p)} - \dfrac{e}{g} + \dfrac{g}{3\times 2^{(1/3)}p} - \left(\dfrac{e}{g} + \dfrac{g}{3\times 2^{(1/3)}p}\right)} - \dfrac{-\frac{q^3}{p^3} + \frac{4qr}{p^2} - \frac{8s}{p}}{4\sqrt{\dfrac{q^2}{(4p^2)} - \dfrac{(2r)}{(3p)} + \dfrac{e}{g} + \dfrac{g}{3\times 2^{(1/3)}p} - \left(\dfrac{e}{g} + \dfrac{g}{3\times 2^{(1/3)}p}\right)}}
\end{cases}
\end{cases}$$

$$e = 2^{(1/3)}(r^2 - 3qs + 12pw)$$

$$g = \left\{3p\left(\frac{2r^3 - 9qrs + 27ps^2 + 27q^2w - 72prw+}{\sqrt{-4(r^2 - 3qs + 12pw)^3 + (2r^3 - 9qrs + 27ps^2 + 27q^2w - 72prw)^2}}\right)^{(1/3)}\right\}$$

References

1. Iijima, S. Helical microtubules of graphitic carbon. *Nature* **1991**, *354*, 56–58. [CrossRef]
2. Mahabaleshwar, U.S.; Sneha, K.N.; Huang, H.-N. An effect of MHD and radiation on CNTS-Water– based nanofluids due to a stretching sheet in a Newtonian fluid. *Case Stud. Therm. Eng.* **2021**, *8*, 101462. [CrossRef]
3. Meyer, J.P.; McKrell, T.J.; Grote, K. The influence of multi-walled carbon nanotubes on single-phase heat transfer and pressure drop characteristics in the transitional flow regime of smooth tubes. *Int. J. Heat Mass Transf.* **2013**, *58*, 597–609. [CrossRef]
4. Li, Q.; Xuan, Y. Convective heat transfer and flow characteristics of Cu–water nanofluid. *Sci. China Ser. E Technolgical Sci.* **2002**, *45*, 408–416.
5. Pak, B.; Cho, Y. Hydrodynamic and heat transfer study of dispersed fluids with submicron metallic oxide particles. *Exp. Heat Transf.* **1998**, *11*, 151–170. [CrossRef]
6. Wen, D.; Ding, Y. Experimental investigation into convective heat transfer ofnanofluids at the entrance region under laminar flow conditions. *Int. J. Heat Mass Transf.* **2004**, *47*, 5181–5188. [CrossRef]
7. Yang, Y.; Zhang, Z.; Grulke, E.; Anderson, W.; Wu, G. Heat transfer properties of nanoparticles-in-fluid dispersions (nanofluids) in laminar flow. *Int. J. Heat Mass Transf.* **2005**, *48*, 1107–1116. [CrossRef]
8. Xie, H.; Lee, H.; Youn, W.; Choi, M. Nanofluids containing multiwalled carbon nanotubes and their enhanced thermal conductivities. *J. Appl. Phys.* **2003**, *94*, 4967–4971. [CrossRef]
9. Khan, M.R.; Pan, K.; Khan, A.U.; Naeem, U. Comparative study on heat transfer in CNTs-water nanofluid over a curved surface. *Int. Commun. Heat Mass Transf.* **2020**, *116*, 104707. [CrossRef]
10. Sneha, K.N.; Mahabaleshwar, U.S.; Chan, A.; Hatami, M. Investigation of radiation and MHD on non-Newtonian fluid flow over a stretching/shrinking sheet with CNTs and mass transpiration. *Waves Random Complex Media* **2022**, 1–20. [CrossRef]
11. Nadeem, S.; Khan, A.U.; Hussain, S.T. Model based study of SWCNT and MWCNT thermal conductivities effect on the heat transfer due to the oscillating wall conditions. *Int. J. Hydrog. Energy* **2017**, *42*, 28945–28957. [CrossRef]
12. Mahabaleshwar, U.S.; Sneha, K.N.; Chan, A.; Zeidan, D. An effect of MHD fluid flow heat transfer using CNTs with thermal radiation and heat source/sink across a stretching/shrinking sheet. *Int. Commun. Heat Mass Transf.* **2022**, *135*, 106080. [CrossRef]
13. Hayat, T.; Nawaz, M.; Sajid, M.; Asghar, S. The effect of thermal radiation on the flow of a second grade fluid. *Comput. Math. Appl.* **2009**, *58*, 369–379. [CrossRef]
14. Devi, S.S.U.; Devi, S.P.A. Numerical Investigation on Three Dimensional Hybrid $Cu-Al_2O_3$/Water Nanofluid Flow Over a Stretching Sheet with Effecting Lorentz Force Subject to Newtonian Heating. *Can. J. Phys.* **2016**, *94*, 490–496. [CrossRef]
15. Bhattacharyya, K.; Layek, G.C. Effects of suction/blowing on steady boundary layer stagnation-point flow and heat transfer towards a shrinking sheet with thermal radiation. *Int. J. Heat Mass Transf.* **2011**, *54*, 302–307. [CrossRef]
16. Bhattacharyya, K.; Mukhopadhyay, S.; Layek, G.C.; Pop, I. Effects of thermal radiation on micropolar fluid flow and heat transfer over a porous shrinking sheet. *Int. J. Heat Mass Transf.* **2022**, *55*, 2945–2952. [CrossRef]
17. Miklavcic, M.; Wang, C.Y. Viscous flow due to a shrinking sheet. *Q. Appl. Math.* **2006**, *64*, 283–290. [CrossRef]
18. Fang, T. Boundary layer flow over a shrinking sheet with power-law velocity. *Int. J. Heat Mass Transf.* **2008**, *51*, 5838–5843. [CrossRef]
19. Wu, L. A slip model for rarefied gas flows at arbitrary Knudsen number. *Appl. Phys. Lett.* **2008**, *93*, 253103. [CrossRef]
20. Wang, C.Y. Analysis of viscous flow due to a stretching sheet with surface slip and suction. *Nonlinear Anal. Real World Appl.* **2009**, *10*, 375–380. [CrossRef]

21. Fang, T.; Yao, S.; Zhang, J.; Aziz, A. Viscous flow over a shrinking sheet with a second order slip flow model. *Commun. Nonlinear Sci. Numer. Simul.* **2010**, *15*, 1831–1842. [CrossRef]
22. Fang, T.; Aziz, A. Viscous Flow with Second-Order Slip Velocity over a Stretching Sheet. *Z. Für Nat. A* **2010**, *65*, 1087–1092. [CrossRef]
23. Wu, L. Mass transfer induced slip effect on viscous gas flows above a shrinking/stretching sheet. *Int. J. Heat Mass Transf.* **2016**, *93*, 17–22. [CrossRef]
24. Wu, L. Effect of mass transfer induced velocity slip on heat transfer of viscous gas flows over stretching/shrinking sheets. *Int. J. Therm. Sci.* **2017**, *112*, 65–173. [CrossRef]
25. Crane, L.J. Flow past a Stretching Plate. *J. Appl. Math. Phys. (ZAMP)* **1970**, *21*, 645–647. [CrossRef]
26. Cortell, R. Flow and heat transfer of a fluid through a porous medium over a stretching surface with internal heat generation/absorption and suction/blowing. *Fluid Dyn. Res.* **2005**, *37*, 231–245. [CrossRef]
27. Bataller, R.C. Similarity solutions for flow and heat transfer of a quiescent fluid over a nonlinearly stretching surface. *J. Mater. Process. Technol.* **2008**, *203*, 176–183. [CrossRef]
28. Mahantesh, M.; Nandeppanavar, K.; Vajravelu, M.; Abel, S.; Ng, C.-O. Heat transfer over a nonlinearly stretching sheet with non-uniform heat source and variable wall temperature. *Int. J. Heat Mass Transf.* **2011**, *54*, 4960–4965. [CrossRef]
29. Mahabaleshwar, U.S.; Aly, E.H.; Vishalakshi, A.B. MHD and Thermal Radiation Flow of Graphene Casson Nanofluid Stretching/Shrinking Sheet. *Int. J. Appl. Comput. Math* **2022**, *8*, 113. [CrossRef]
30. Anusha, T.; Mahabaleshwar, U.S.; Sheikhnejad, Y. An MHD of Nanofluid Flow over a Porous Stretching/Shrinking Plate with Mass Transpiration and Brinkman Ratio. *Transp. Porous Med.* **2022**, *142*, 333–352. [CrossRef]
31. Vishalakshi, A.B.; Mahabaleshwar, U.S.; Sarris, I.E. An MHD Fluid Flow over a Porous Stretching/Shrinking Sheet with Slips and Mass Transpiration. *Micromachines* **2022**, *13*, 116. [CrossRef] [PubMed]
32. Sneha, K.N.; Mahabaleshwar, U.S.; Sharifpur, M.; Ahmadi, M.H.; Al-Bahrani, M. Entropy Analysis in MHD CNTS Flow Due to a Stretching Surface with Thermal Radiation and Heat Source/Sink. *Mathematics* **2022**, *10*, 3404. [CrossRef]
33. Areekara, S.; Sabu, A.S.; Kumar, R.; Mathew, A. Triple stratification effects on bioconvective stagnation point flow pertaining carbon nanotubes due to induced magnetic field. *ZAMM-J. Appl. Math. Mech./Z. Für Angew. Math. Und Mech.* **2021**, *101*, e202000375. [CrossRef]
34. Reddy, Y.R.O.; Reddy, M.S.; Reddy, P.S. MHD boundary layer flow of SWCNT-water and MWCNT-water nanofluid over a vertical cone with heat generation/absorption. *Heat Transf.-Asian Res.* **2019**, *48*, 539–555. [CrossRef]
35. Samantaray, S.S.; Shaw, S.; Misra, A.; Nayak, M.K.; Prakash, J. Darcy–Forchheimer up/downflow of entropy optimized radiative nanofluids with second-order slip, nonuniform source/sink, and shape effects. *Heat Transf.* **2022**, *51*, 2318–2342. [CrossRef]
36. Muhammad, T.; Waqas, H.; Farooq, U.; Alqarni, M.S. Numerical simulation for melting heat transport in nanofluids due to quadratic stretching plate with nonlinear thermal radiation. *Case Stud. Therm. Eng.* **2021**, *27*, 101300. [CrossRef]
37. Mathew, A.; Areekara, S.; Sabu, A.S.; Saleem, S. Significance of multiple slip and nanoparticle shape on stagnation point flow of silver-blood nanofluid in the presence of induced magnetic field. *Surf. Interfaces* **2021**, *25*, 101267. [CrossRef]
38. Ullah, K.W.; Awais, M.; Parveen, N.; Ali, A.; Awan, S.E.; Malik, M.Y.; He, Y. Analytical Assessment of (Al_2O_3–Ag/H_2O) Hybrid Nanofluid Influenced by Induced Magnetic Field for Second Law Analysis with Mixed Convection, Viscous Dissipation and Heat Generation. *Coatings* **2021**, *11*, 498. [CrossRef]
39. Khan, U.; Zaib, A.; Ishak, A.; Bakar, S.A. Time-dependent Blasius–Rayleigh–Stokes flow conveying hybrid nanofluid and heat transfer induced by non-Fourier heat flux and transitive magnetic field. *Case Stud. Therm. Eng.* **2021**, *26*, 101151. [CrossRef]
40. Panigrahi, L.; Panda, J.; Sahoo, S.S. Unsteady Heat Transfer and Entropy Generation Study on Viscoelastic Fluid Flow Coupled with Induced Magnetic Field. *Iran. J. Sci. Technol. Trans. Sci.* **2021**, *45*, 1699–1710. [CrossRef]
41. Schlichting, H. *Boundary-Layer Theory*; Springer: Berlin/Heidelberg, Germany, 2004; ISBN 978-3-540-66270-9.
42. Khan, W.A.; Khan, Z.H.; Rahi, M. Fluid flow and heat transfer of carbon nanotubes along a flat plate with Navier slip boundary. *Appl. Nanosci.* **2014**, *4*, 633–641. [CrossRef]
43. Alexander, B.; Michael, N. Einstein's viscosity equation and nanolubricated friction. *Langmuir* **2018**, *34*, 12968–12973. [CrossRef]
44. Xue, Q.Z. Model for thermal conductivity of carbon nanotube-based composites. *Phys. B Condens. Matter* **2005**, *368*, 302–307. [CrossRef]
45. Chereches, E.I.; Minea, A.A. Electrical Conductivity of New Nanoparticle Enhanced Fluids: An Experimental Study. *Nanomaterials* **2019**, *9*, 1228. [CrossRef]